Cell Biology

AXONAL distribution of mitochondria maintains neuronal autophagy during aging via eIF2β

Reviewed Preprint
v2 • January 23, 2025
Revised by authors

Reviewed Preprint
v1 • March 25, 2024

Kanako Shinno, Yuri Miura, Koichi M Iijima, Emiko Suzuki, Kanae Ando

Department of Biological Sciences, Graduate School of Science, Tokyo Metropolitan University, Tokyo, Japan • Research Team for Mechanism of Aging, Tokyo Metropolitan Institute for Geriatrics and Gerontology, Tokyo, Japan • Department of Alzheimer's Disease Research, National Center for Geriatrics and Gerontology, Ōbu, Japan • Department of Experimental Gerontology, Graduate School of Pharmaceutical Sciences, Nagoya City University, Nagoya, Japan • Gene Network Laboratory, National Institute of Genetics and Department of Genetics, Mishima, Japan • Department of Biological Sciences, School of Science, Tokyo Metropolitan University, Tokyo, Japan

eLife Assessment

In flies defective for axonal transport of mitochondria, the authors report the upregulation of one subunit, the beta subunit, of the heterotrimeric eIF2 complex via mass spectroscopy proteome analysis. Neuronal overexpression of eIF2β phenocopied aspects of neuronal dysfunction observed when axonal transport of mitochondria was compromised. Conversely, lowering eIF2β expression suppressed aspects of neuronal dysfunction. While these are intriguing, potentially **useful** observations, several technical weaknesses limit the interpretation and mean the evidence supporting the current claims is **incomplete**.

https://doi.org/10.7554/eLife.95576.2.sa3

Abstract

Summary

Neuronal aging and neurodegenerative diseases are accompanied by proteostasis collapse, while cellular factors that trigger it are not identified. Impaired mitochondrial transport in the axon is another feature of aging and neurodegenerative diseases. Using *Drosophila*, we found that genetic depletion of axonal mitochondria causes dysregulation of protein degradation. Axons with mitochondrial depletion showed abnormal protein accumulation and autophagic defects. Lowering neuronal ATP levels by blocking glycolysis did not reduce autophagy, suggesting that autophagic defects are associated with mitochondrial distribution. We found that eIF2β was increased by the depletion of axonal mitochondria via proteome analysis. Phosphorylation of eIF2α, another subunit of eIF2, was lowered, and global translation was suppressed. Neuronal overexpression of *eIF2β* phenocopied the autophagic defects and neuronal dysfunctions, and lowering *eIF2β* expression rescued those perturbations caused by depletion of axonal mitochondria. These results indicate the

mitochondria-eIF2β axis maintains proteostasis in the axon, of which disruption may underly the onset and progression of age-related neurodegenerative diseases.

Highlights

- Loss of axonal mitochondria impairs autophagy and accumulates proteins in the axon
- Loss of axonal mitochondria increases eIF2β and decreases p-eIF2α
- Neuronal upregulation of eIF2β induces autophagic defects and locomotor dysfunction
- Lowering eIF2β rescues autophagic defects caused by loss of axonal mitochondria

Introduction

Neurons have a morphologically complex architecture composed of microcompartments and require tight regulation of the abundance of proteins and organelles spatially and temporally[1]. Such control of protein amounts, or proteostasis, is essential for neuronal functions[2] and is achieved through the orchestration of protein expression, folding, trafficking, and degradation controlled by intrinsic and environmental signals[3]. Translation is initiated by the eukaryotic initiation factor 2 (eIF2) complex[4]. eIF2, a heterotrimer of α, β, and γ subunits, transports Met-tRNA to the ribosome in a GTP-dependent manner[5]. Under stressed conditions, phosphorylation of eIF2α attenuates global translation and initiates translation of mRNAs related to the integrated stress response (ISR)[6]. As for protein degradation, autophagy and proteasome are major systems that maintain proteostasis[7]. The proteasome degrades unnecessary proteins, followed by regulated ubiquitination processes[8], and autophagy removes damaged or harmful components, including large protein aggregates and organelles, through catabolism (selective autophagy)[9]. In addition to autophagy induced by acute stressors, a basal level of selective autophagy mediates the global turnover of damaged proteins[10].

Such constitutive autophagy decreases during aging, which may underlie declines in the structural and functional integrity of neurons[11]. Decreased protein degradation and accumulation of abnormal proteins also contribute to increased risks of neurodegenerative diseases. Age-related neurodegenerative diseases such as Alzheimer's disease and Parkinson's disease are often associated with the accumulation of misfolded proteins such as amyloid-β, tau, and α-synuclein[12]. Enhancement of autophagy mitigates age-related dysfunctions and neurodegeneration caused by proteotoxic stress[13]. However, it is not fully understood how aging disrupts the regulation of this constitutive autophagy.

Neurons are also highly energy-demanding cells. At nerve terminals, action potentials trigger the release of neurotransmitters via exocytosis of synaptic vesicles, which requires a constant supply of ATP and calcium buffering[14]. Such neuronal activity relies on mitochondrial functions[15], and mitochondria are actively transported from their major sites of biogenesis in soma to axons[16]. However, the axonal transport of mitochondria declines during aging[17,18,19]. Reduced axonal transport of mitochondria is thought to contribute to age-related declines in neuronal functions[17,19,20,21]. The number of functional mitochondria in synapses is reduced in the brains of patients suffering from age-related neurodegenerative diseases such as Alzheimer's disease[22], and mutations in genes involved in mitochondrial dynamics are linked to neurodegenerative diseases[23]. The mislocalization of mitochondria is sufficient to cause age-dependent neurodegeneration in *Drosophila* and mice[24,25], indicating that the proper

distribution of mitochondria is essential to maintain neuronal functions. Thus, depletion of functional mitochondria from axons and proteostasis collapse are common features of aging and neurodegenerative diseases.

Mitochondrial transport is regulated by a series of molecular adaptors that mediate the attachment of mitochondria to molecular motors[16]. In *Drosophila*, mitochondrial transport is mediated by milton and Miro, which attaches mitochondria to microtubules via kinesin heavy chain[26,27]. In the absence of milton or Miro, synaptic terminals and axons lack mitochondria, although mitochondria are numerous in the neuronal cell body[28]. We previously reported that RNAi-mediated knockdown of *milton* or *Miro* in neurons causes a reduction in axonal mitochondria, age-dependent locomotor defects[29], and age-dependent neurodegeneration in neuropile area starting around 30 days after eclosion (day-old)[24]., and enhances axon degeneration caused by human tau proteins[24], suggesting that these flies can be used as a model to analyze the effect of depletion of axonal mitochondria during aging. In this study, we investigated a causal relationship between mitochondrial distribution and neuronal proteostasis by using neuronal knockdown of *milton*. We found that depletion of axonal mitochondria reduced autophagy and increased the accumulation of aggregated proteins in the axon prior to gross neurodegeneration. Proteome analysis and follow-up biochemical analyses revealed that neuronal knockdown of *milton* increased eIF2β levels and lowered phosphorylation of eIF2αin the axon. In addition, *milton* knockdown suppressed global translation. Overexpression of *eIF2β* was sufficient to decrease autophagy and induce neuronal dysfunction, and genetic suppression of *eIF2β* restored autophagy and improved neuronal function in the *milton* knockdown background. These findings suggest that loss of axonal mitochondria and elevated levels of eIF2β mediate proteostasis collapse and neuronal dysfunction during aging.

Results

Depletion of axonal mitochondria by knockdown of *milton* or *Miro* causes protein accumulation in the axon

In *Drosophila*, mitochondrial transport is mediated by milton and Miro, which attach mitochondria to microtubules via kinesin heavy chain[26,27] (**Figure 1A**). It has been reported that expression of *milton* RNAi in neurons via pan-neuronal elav-GAL4 driver reduced milton protein levels in *Drosophila* head lysate to 40% and mito-GFP signals in axons to 50%[24,29].

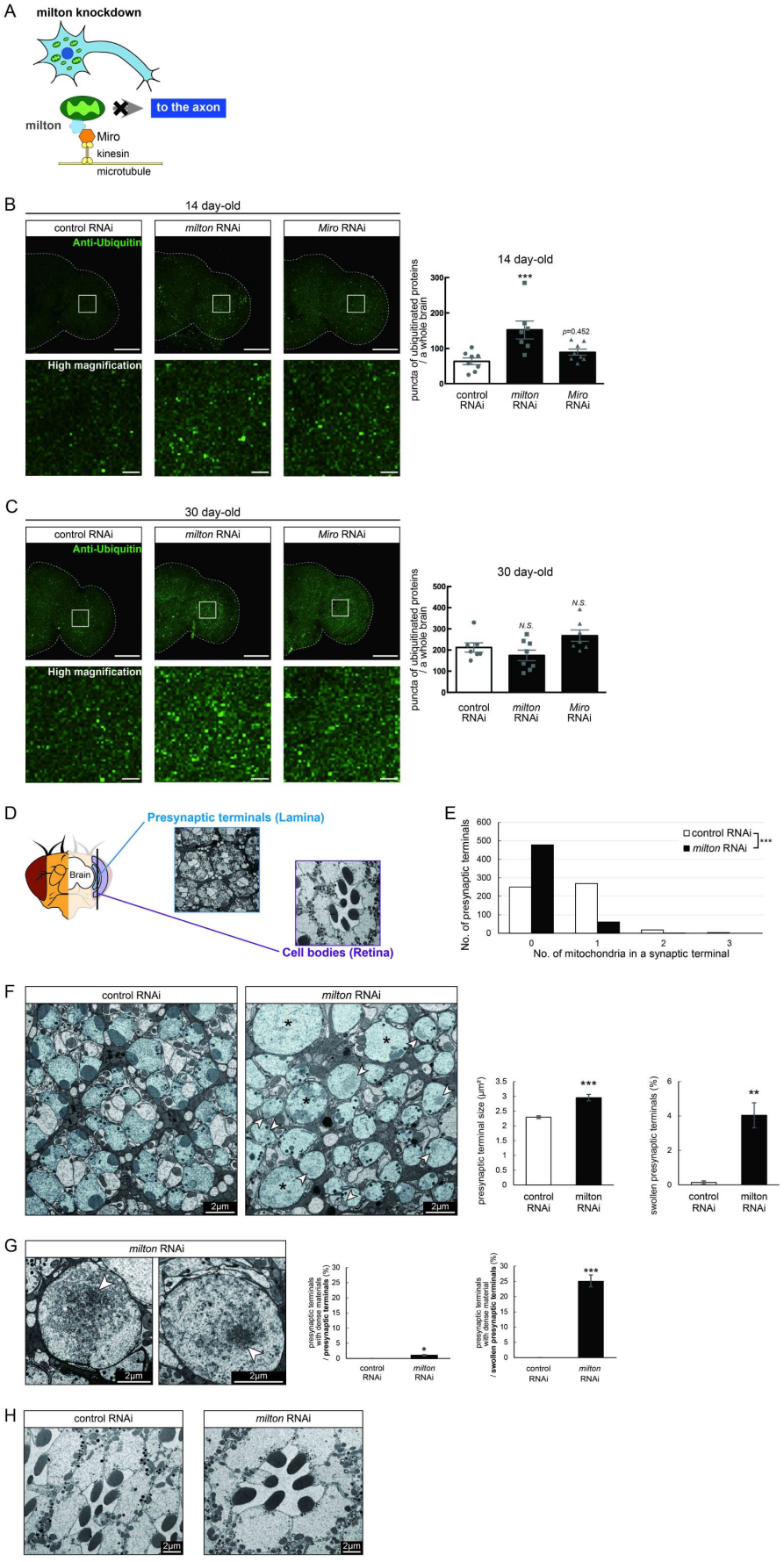
A
milton knockdown
to the axon
milton
Miro
kinesin
microtubule
B
14 day-old
control RNAi
milton RNAi
Miro RNAi
Anti-Ubiquitin
High magnification
puncta of ubiquitinated proteins / a whole brain
***
p=0.452
control RNAi
milton RNAi
Miro RNAi
C
30 day-old
N.S.
D
Presynaptic terminals (Lamina)
Brain
Cell bodies (Retina)
E
control RNAi
milton RNAi
***
No. of presynaptic terminals
No. of mitochondria in a synaptic terminal
F
presynaptic terminal size (μm²)
swollen presynaptic terminals (%)
**
2μm
G
presynaptic terminals with dense materials / presynaptic terminals (%)
presynaptic terminals with dense materials / swollen presynaptic terminals (%)
H

Figure 1.

Knockdown of *milton* or *Miro* causes protein accumulation in the axon

(A) Schematic representation of the mitochondrial transport machinery. Knockdown of *milton*, an adapter protein for mitochondrial transport, depletes mitochondria in the axon. (B, C) Ubiquitinated proteins in brains with neuronal knockdown of *milton* or *Miro*. Brains dissected at 14-day-old (B) or 30-day-old (C) were immunostained with an antibody against ubiquitin. Firefly *luciferase* RNAi was used as a control. Representative images (left) and quantitation of the number of ubiquitin-positive puncta (right) are shown. Scale bars of hemibrains, 100 μm, Scale bars of high magnifications, 10 μm. Means ± SE, n = 8. *N.S.*, $p > 0.05$; ***$p < 0.005$ (one-way analysis of variance (ANOVA) followed by Tukey's honestly significant difference (HSD) *post hoc* test). (D) Cross sections in the lamina and in the retina were used to analyze the ultrastructure of synapses and cell bodies, respectively. *milton* RNAi was expressed in the retina and neurons via a combination of GAL4 drivers, a pan-retinal gmr-GAL4 and pan-neuronal elav-GAL4. (E) Quantitation of the number of mitochondria in a presynaptic terminal from transmission electron micrographs. 180 presynaptic terminals from cross-sections of the lamina from three brains were analyzed. ***$p < 0.005$ (Chi-square test). (F, G) Presynaptic terminals of photoreceptor neurons of control and *milton* knockdown flies. Photoreceptor neurons are highlighted in blue. Swollen presynaptic terminals (asterisks in (F)), characterized by the enlargement and higher circularity, were found more frequently in *milton* knockdown neurons. Arrowheads indicate presynaptic terminals with dense materials. Scale bars, 2 μm. Representative images (Left) and quantitation (Right) are shown. 918–1118 from three heads were quantified for the percentage of swollen presynaptic terminals, and 180 presynaptic terminals from three heads were quantified for the size of presynaptic terminals. Mean ± SE, **$p < 0.01$, ***$p < 0.005$ (Student's *t*-test). (G) Dense materials (arrowheads in (G)) in the presynaptic terminals of *milton* knockdown neurons. Scale bars, 2 μm. The ratio of presynaptic terminals containing dense materials were quantified from 918–1118 presynaptic terminals from three heads. Mean ± SE, ***$p < 0.005$ (Student's *t*-test). (H) Cell bodies of photoreceptor neurons of control and *milton* knockdown flies. Scale bars, 2 μm. Flies were 27-day-old.

To test how loss of axonal mitochondria affects proteostasis in neurons, we first examined the accumulation of ubiquitinated proteins. At 14 day-old, more ubiquitinated proteins were deposited in the brains of *milton* knockdown flies than in those of age-matched control flies (**Figure 1B**, $p < 0.005$ between control RNAi and *milton* RNAi). There was no significant increase in ubiquitinated proteins in *milton* knockdown flies at 1-day old, suggesting that the accumulation of ubiquitinated proteins caused by *milton* knockdown is age-dependent (Figure S1). We also analyzed the effect of the neuronal knockdown of *Miro*, a partner of milton, on the accumulation of ubiquitin-positive proteins. Since severe knockdown of *Miro* in neurons causes lethality, we used UAS-*Miro* RNAi strain with low knockdown efficiency, whose expression driven by elav-GAL4 caused 30% reduction of *Miro* mRNA in head extract[24]. Although there was a tendency for increased ubiquitin-positive puncta in *Miro* knockdown brains, the difference was not significant (**Figure 1B**, $p>0.05$ between control RNAi and *Miro* RNAi). These data suggest that the depletion of axonal mitochondria induced by *milton* knockdown leads to the accumulation of ubiquitinated proteins before neurodegeneration occurs.

It has been reported that ubiquitinated proteins accumulate with aging[30]; thus, we analyzed the accumulation of ubiquitinated proteins in aged brains (30 day-old) with *milton* knockdown. The number of puncta of ubiquitinated proteins did not significantly differ between control and *milton* knockdown flies or between control and *Miro* knockdown flies (**Figure 1C**, $p > 0.05$). These results suggest that depletion of axonal mitochondria may have more impact on proteostasis in young neurons than in old neurons. We examined the ultrastructure of presynaptic terminals and cell bodies in photoreceptor neurons with *milton* knockdown by transmission electron microscopy in 27-day-old flies (**Figure 1D**). As previously reported[24], the number of mitochondria in presynaptic terminals decreased in *milton* knockdown (**Figure 1E**). The swelling of presynaptic terminals, characterized by the enlargement and roundness, was not reported at 3-day-old[24] but observed at this age with about 4% of total presynaptic terminals (**Figure 1F**, asterisks).

Some presynaptic terminals of *milton* knockdown neurons contained dense materials (**Figure 1F** and **G**, arrowheads). Dense materials are rarely found in age-matched control neurons, indicating that *milton* knockdown induces abnormal protein accumulation in the presynaptic terminals (**Figure 1G** and **H**). In *milton* knockdown neurons, dense materials are found in swollen presynaptic terminals more often than in presynaptic terminals without swelling, suggesting a positive correlation between the disruption of proteostasis and axonal damage (**Figure 1G**). In contrast, dense materials were not observed in cell bodies in the *milton* knockdown retina (**Figure 1H**). These results indicate that the depletion of axonal mitochondria induces protein accumulation in the axon.

Depletion of axonal mitochondria impairs protein degradation pathways

Since abnormal proteins were accumulated in *milton* knockdown brains, we next examined if protein degradation pathways were suppressed. We analyzed autophagy via western blotting of the autophagy markers LC3 and p62[31]. During autophagy progression, LC3 is conjugated with phosphatidylethanolamine to form LC3-II, which localizes to isolation membranes and autophagosomes. LC3-I accumulation occurs when autophagosome formation is impaired, and LC3-II accumulation is associated with lysosomal defects[31,32]. p62 is an autophagy substrate, and its accumulation suggests autophagic defects[31,32]. We found that *milton* knockdown increased LC3-I, and the LC3-II/LC3-I ratio was lower in *milton* knockdown flies than in control flies at 14-day-old (**Figure 2A**). We also analyzed p62 levels in head lysates sequentially extracted using detergents with different stringencies (1% Triton X-100 and 2% SDS). Western blotting revealed that p62 levels were increased in the brains of 14-day-old of *milton* knockdown flies (**Figure 2B**). The increase in the p62 level was significant in the Triton X-100-soluble fraction but not in the SDS-soluble fraction (**Figure 2B**), suggesting that depletion of axonal mitochondria impairs the degradation of less-aggregated proteins. Proteasome activity was also significantly decreased in brains with neuronal knockdown of *milton* (**Figure 2C**, $p < 0.005$).

At 30 day-old, LC3-I was still higher, and the LC3-II/LC3-I ratio was lower, in *milton* knockdown compared to the control (**Figure 2D**). At this age, *milton* knockdown increased p62 significantly in 1% Triton X-100 fraction and 2% SDS fraction (**Figure 2E**). Proteasome activities were also decreased in *milton* knockdown flies at 30-day-old (**Figure 2F**). These results indicate that depletion of axonal mitochondria impairs protein degradation pathways.

ATP deprivation does not impair autophagy

milton knockdown downregulates ATP in the axon[33]. To examine whether the disruption of protein degradation pathways by *milton* knockdown is due to ATP deprivation, we investigated the effects of knocking down phosphofructokinase (*Pfk*), a rate-limiting enzyme in glycolysis, on protein degradation pathways. Neuronal knockdown of *Pfk* was reported to lower ATP levels in brain neurons[33]. *Pfk* knockdown and *milton* knockdown decreased ATP to similar levels (**Figure 3A-C**). However, in contrast with *milton* knockdown, *Pfk* knockdown did not affect the levels of LC3-I, LC3-II or the LC3-II/LC3-I ratio (**Figure 3D**). *Pfk* knockdown decreased p62 level (**Figure 3E**), suggesting that autophagy is promoted. On the other hand, proteasome activity was decreased by *Pfk* knockdown (**Figure 3F**). These results suggest that the downregulation of axonal ATP upon depletion of axonal mitochondria decreases proteasome activity, but not autophagy.

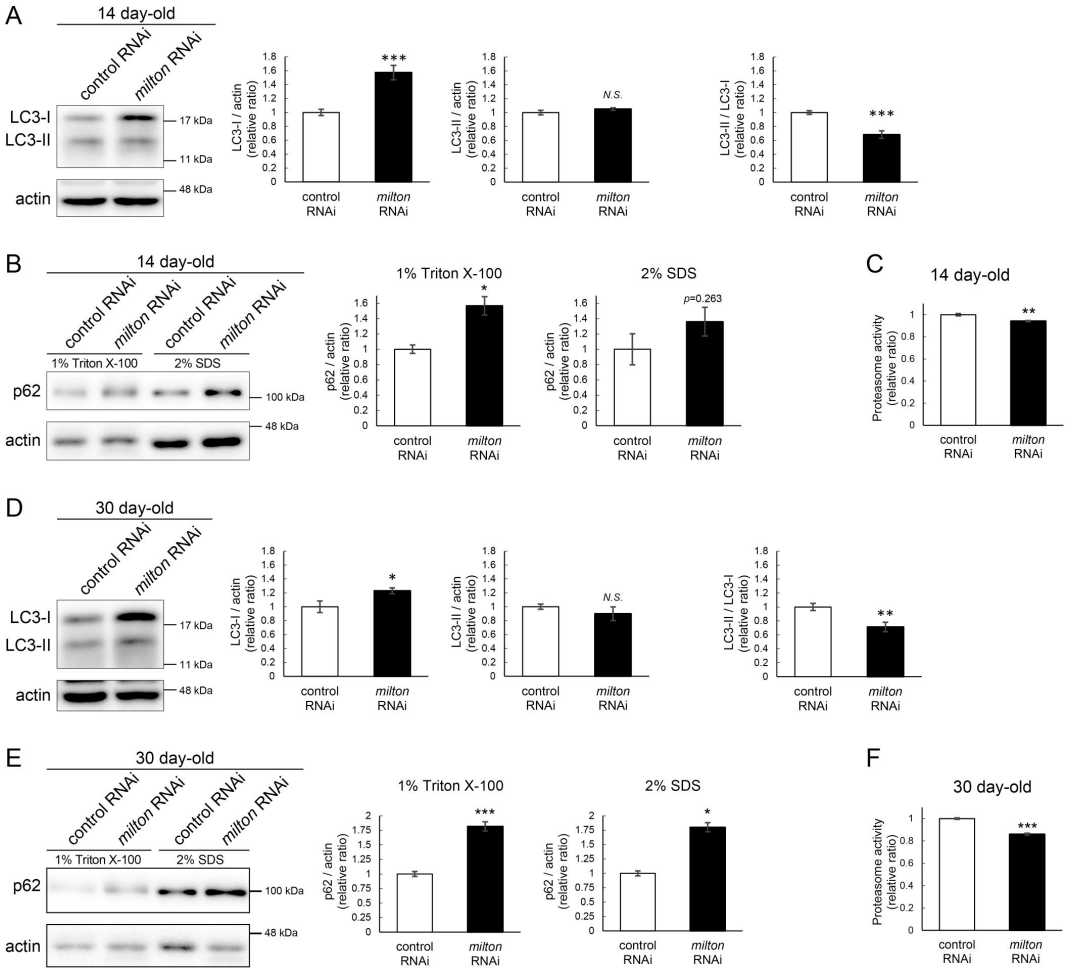

Figure 2.

milton knockdown impairs protein degradation pathways

(A, B) Western blotting of head extracts of control and *milton* knockdown flies with antibodies against LC3 (A) and Ref2P, the fly homolog of mammalian p62 (B). For the analyses of p62 levels, heads were extracted with 1% Triton X-100 or 2% SDS (B). Flies were 14-day-old. Representative blots (left) and quantitation (right) are shown. Actin was used as a loading control. Means ± SE, n = 6 (LC3), n = 3 (p62). (C) Proteasome activity in head extracts of control and *milton* knockdown flies was measured by hydrolysis of Suc-LLVY-AMC at 14-day-old. Means ± SE, n = 3. (D, E) Western blotting of head extracts of 30-day-old control and *milton* knockdown flies. Blotting was performed with anti-LC3 (D) and anti-p62 (E) antibodies. Representative blots (left) and quantitation (right) are shown. Actin was used as a loading control. Means ± SE, n = 6 (LC3), n = 3 (p62). (F) Proteasome activity in head extracts of 30-day-old control and *milton* knockdown flies. Means ± SE, n = 3. *N.S.*, $p > 0.05$; *$p < 0.05$; **$p < 0.01$; ***$p < 0.005$ (Student's *t*-test).

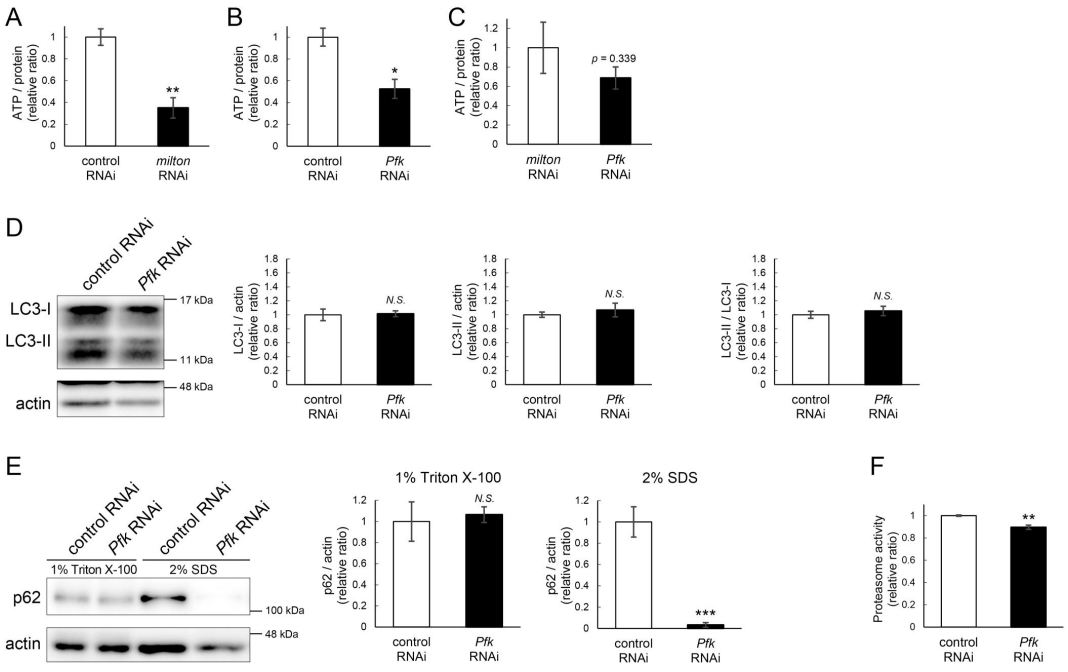

Figure 3.

ATP deprivation does not impair autophagy

(A-C) ATP levels in brain extracts of control and *milton* knockdown flies (A) and control and *Pfk* knockdown flies (B) and comparison of the effects of *milton* knockdown and *Pfk* knockdown on ATP levels (C). Flies were 14 day-old. Means ± SE, n = 3. (D, E) Western blotting of head extracts of flies with neuronal expression of control or *Pfk* RNAi. Blotting was performed with anti-LC3 (D) and anti-p62 (E) antibodies. For analyses of p62 levels, heads were extracted with 1% Triton X-100 or 2% SDS. Representative blots (left) and quantitation (right) are shown. Actin was used as a loading control. Means ± SE, n = 6 (LC3), n = 3 (p62). (F) Proteasome activity in head lysates of flies with neuronal expression of control or *Pfk* RNAi was measured by hydrolysis of Suc-LLVY-AMC. Means ± SE, n = 3. *N.S.*, $p > 0.05$; *$p < 0.05$; **$p < 0.01$; ***$p < 0.005$ (Student's *t*-test). Flies were at 14 day-old.

Proteome analysis suggests that depletion of axonal mitochondria causes disruption of autophagy and premature aging

To identify the pathways that mediate the decrease in autophagy in *milton* knockdown brains, we performed proteome analysis to systematically detect differentially expressed proteins upon neuronal knockdown of *milton*. We analyzed flies at 7- and 21-day-old, the age before autophagic defects are detected and the age just before the onset of neurodegeneration, respectively (**Figure 4A**). 1039 proteins were detected by liquid chromatography-tandem mass spectrometry (LC-MS/MS). Expression of 36 proteins was significantly increased (22 proteins) or decreased (14 proteins) by *milton* knockdown at 7-day-old (**Figure 4B**, **Tables 1** and S1). At 21 day-old, the expression of 41 proteins (31 upregulated and ten downregulated proteins) was significantly altered in *milton* knockdown flies compared with control flies (**Figure 4C**, **Tables 1** and S1). The “Interaction search” algorithm using KeyMolnet showed that proteins whose expression was significantly altered in the brains of *milton* knockdown flies at both 7- and 21-day-old were closely associated with the autophagic pathway (**Table 2**). Proteins involved in pathways characteristics of aging, such as the immune response (Transcriptional regulation by STAT), cancer (Transcriptional regulation by SMAD, Transcriptional regulation by myc), longevity (Transcriptional regulation by FOXO, Sirtuin signaling pathway), and stress responses (HSP90 signaling pathway, MAPK signaling pathway)[34,35], were enriched in the proteome profiles of *milton* knockdown flies compared with those of control flies at 7-day-old (**Table 2**), suggesting that depletion of axonal mitochondria accelerates aging in the brain.

7 day-old

Accession[a]	Name	Abundance Ratio: (7 days, milton KD) / (7 days, control)	Abundance Ratio P-Value: (7 days, milton KD) / (7 days, control)
Q9V751	Attacin-B	100	1E-17
Q04448	Bifunctional methylenetetrahydrofolate dehydrogenase/cyclohydrolase, mitochondrial	100	1E-17
P22700	Calcium-transporting ATPase sarcoplasmic/endoplasmic reticulum type	100	1E-17
Q9V558	Cytochrome P450 4p1	100	1E-17
P10552	FMRFamide-related peptides	100	1E-17
P05661-19	Isoform F of Myosin heavy chain, muscle	100	1E-17
Q9VE01	Probable cytochrome P450 12a5, mitochondrial	100	1E-17
Q7KIN0	Toll-like receptor 7	100	1E-17
Q8MKN0	Ubiquinone biosynthesis protein COQ9, mitochondrial	100	1E-17
Q9VJG0	Xaa-Pro aminopeptidase ApepP	100	1E-17
Q9V8F5	Bomanin Bicipital 1	4.908	1E-17
P07701	Salivary glue protein Sgs-5	2.843	1.99252E-09
O76902	Pleckstrin homology domain-containing family F member 1 homolog	2.836	2.22045E-16
P81641	Alpha-amylase B	2.684	7.44847E-09
P19351-4	Isoform 4 of Troponin T, skeletal muscle	2.66	6.65563E-11
Q9VTJ8	Mitochondrial import inner membrane translocase subunit TIM14	2.61	3.54205E-07
P41375	Eukaryotic translation initiation factor 2 subunit 2	2.465	3.38486E-09
Q9VYB0	Selenoprotein BthD	2.462	2.25579E-08
B7Z0W9	Proton channel OtopLc	2.382	1.71741E-06
Q9VLR5	RNA polymerase II transcriptional coactivator	2.245	6.70245E-09
Q8IN44	Protein Turandot A	2.127	8.38662E-13
P27779	Pupal cuticle protein Edg-78E	2.113	1.00215E-08
Q9W1X8	Probable GDP-L-fucose synthase	0.496	2.12601E-08
P55035	26S proteasome non-ATPase regulatory subunit 4	0.487	5.50158E-11
Q9VHN6	39S ribosomal protein L19, mitochondrial	0.487	0.000551337
Q9VPD2	Cytosolic Fe-S cluster assembly factor NUBP2 homolog	0.46	6.34514E-05
Q9VHD3	Probable maleylacetoacetate isomerase 1	0.432	4.50956E-06
Q94529	Probable pseudouridine-5'-phosphatase	0.416	1.08802E-14
Q27606	Cytochrome P450 4e2	0.398	4.13128E-10
Q24388	Larval serum protein 2	0.378	1.33227E-14
Q9VKH6	Lysosomal thioesterase PPT2 homolog	0.369	2.05225E-06
Q24114	Division abnormally delayed protein	0.307	2.24406E-09
Q95NH6	Attacin-C	0.01	1E-17
P29993	Inositol 1,4,5-trisphosphate receptor	0.01	1E-17
Q94526	Open rectifier potassium channel protein 1	0.01	1E-17
Q9Y115	UNC93-like protein	0.01	1E-17

[a] UniProt accession number

21 day-old

Accession[a]	Name	Abundance Ratio: (21 days, Milton KD) / (21 days, Control)	Abundance Ratio P-Value: (21 days, Milton KD) / (21 days, Control)
Q10714	Angiotensin-converting enzyme	100	1E-17
C0HKQ8	Cecropin-A2	100	1E-17
Q9V558	Cytochrome P450 4p1	100	1E-17
P51592	E3 ubiquitin-protein ligase hyd	100	1E-17
Q9VMJ7	Lysine-specific demethylase lid	100	1E-17
Q9VXP4	Platelet-activating factor acetylhydrolase IB subunit beta homolog	100	1E-17
Q9VY28	Probable 28S ribosomal protein S25, mitochondrial	100	1E-17
Q9W391	Probable phosphorylase b kinase regulatory subunit alpha	100	1E-17
Q9VUQ5	Protein argonaute-2	100	1E-17
P54359	Septin-2	100	1E-17
P24492	Diptericin A	15.716	1E-17
Q9VVY3	Glycogen-binding subunit 76A	8.986	1E-17
Q70PY2	Peptidoglycan-recognition protein SB1	6.669	1E-17
Q9W0M1	Centrosomal protein cep290	6.526	1E-17
P81641	Alpha-amylase B	5.722	1E-17
P45884	Attacin-A	4.997	1E-17
C0HL66	Histone H3.3A	4.778	1E-17
P26675	Protein son of sevenless	4.696	1E-17
P02515	Heat shock protein 22	4.69	1E-17
Q95NH6	Attacin-C	4.35	1E-17
P17971-1	Isoform A of Potassium voltage-gated channel protein Shal	4.195	1E-17
Q7K1U0	Activity-regulated cytoskeleton associated protein 1	3.271	1E-17
P14199	Protein ref(2)P	3.014	1E-17
Q9VU02	Probable small nuclear ribonucleoprotein Sm D1	2.43	4.91607E-13
Q9VD44	Poly(A) RNA polymerase gld-2 homolog A	2.268	2.6084E-11
Q9V8F5	Bomanin Bicipital 1	2.24	5.16671E-11
P22979	Heat shock protein 67B3	2.223	7.90048E-11
P27779	Pupal cuticle protein Edg-78E	2.192	1.65944E-10
Q9NBK5	Serine/threonine-protein kinase tricornered	2.059	4.15071E-09
Q8MLZ7	Chitinase-like protein Idgf3	2.055	4.61182E-09
Q9V751	Attacin-B	2.038	6.79416E-09
Q9V8M5	Probable 3-hydroxyisobutyrate dehydrogenase, mitochondrial	0.492	7.42952E-09
P84345	ATP synthase protein 8	0.421	1.809E-12
P33438	Glutactin	0.414	6.13731E-13
Q8IN44	Protein Turandot A	0.218	1E-17
Q8IN43	Protein Turandot C	0.195	1E-17
Q9VFI9	cGMP-specific 3',5'-cyclic phosphodiesterase	0.01	1E-17
Q94526	Open rectifier potassium channel protein 1	0.01	1E-17
Q9VHD3	Probable maleylacetoacetate isomerase 1	0.01	1E-17
Q9W0A0	Protein draper	0.01	1E-17
A1Z7T0	Serine/threonine-protein kinase N	0.01	1E-17

7 day-old					
Rank	Name	Score	Score (p) [a]	Score (v) [b]	Score (c) [c]
1	Autophagy-related protein signaling pathway	50.394	6.76E-16	0.159	0.11
2	Calcium signaling pathway	47.583	4.75E-15	0.146	0.117
3	Transcriptional regulation by SMAD	44.012	5.64E-14	0.146	0.095
4	GABA signaling pathway	40.706	5.58E-13	0.122	0.123
5	estrogen signaling pathway	37.507	5.12E-12	0.11	0.13
6	Sirtuin signaling pathway	36.87	7.96E-12	0.122	0.095
7	Transcriptional regulation by AP-1	34.874	3.18E-11	0.11	0.107
8	Arrestin signaling pathway	32.84	1.30E-10	0.11	0.092
9	G protein (Gq/11) signaling pathway	30.889	5.03E-10	0.085	0.149
10	Kainate receptor signaling pathway	30.049	9.00E-10	0.073	0.214
11	Transcriptional regulation by C/EBP	29.5	1.32E-09	0.098	0.093
12	Calpain signaling pathway	28.597	2.46E-09	0.11	0.066
13	Phospholipase D signaling pathway	28.344	2.94E-09	0.098	0.084
14	HSP90 signaling pathway	27.188	6.54E-09	0.085	0.104
14	CYP family	27.188	6.54E-09	0.085	0.104
16	Kir3 channel signaling pathway	26.495	1.06E-08	0.061	0.25
17	Estrogen biosynthesis	26.107	1.38E-08	0.061	0.238
18	CaSR signaling pathway	25.39	2.27E-08	0.061	0.217
19	PI3K signaling pathway	24.927	3.14E-08	0.073	0.122
20	PAF receptor signaling pathway	24.555	4.06E-08	0.049	0.4
21	Transcriptional regulation by PPARa	24.398	4.52E-08	0.073	0.115
21	BTK signaling pathway	24.398	4.52E-08	0.073	0.115
23	Transcriptional regulation by STAT	24.076	5.66E-08	0.085	0.077
24	G protein (Gi/o) signaling pathway	24.063	5.71E-08	0.073	0.111
25	PARP signaling pathway	23.742	7.13E-08	0.073	0.107
25	mGluR signaling pathway	23.742	7.13E-08	0.073	0.107
27	Free fatty acid signaling pathway	23.433	8.83E-08	0.073	0.103
28	Kir channel signaling pathway	23.338	9.43E-08	0.061	0.167
29	Oxytocin signaling pathway	23.327	9.51E-08	0.049	0.333
30	Transcriptional regulation by MEF2	22.99	1.20E-07	0.073	0.098
31	S100 family signaling pathway	22.434	1.77E-07	0.073	0.092
32	Transcriptional regulation by FOXO	22.301	1.94E-07	0.073	0.091
33	P2Y signaling pathway	22.172	2.12E-07	0.061	0.143
34	Transcriptional regulation by SRF	21.174	4.23E-07	0.061	0.125
34	ATF4/ATF6/IRE1 signaling pathway	21.174	4.23E-07	0.061	0.125
36	Chemerin signaling pathway	21.082	4.50E-07	0.049	0.235
36	Vasopressin signaling pathway	21.082	4.50E-07	0.049	0.235
38	Serotonin signaling pathway	20.854	5.28E-07	0.073	0.077
39	Transcriptional regulation by HIF	20.834	5.35E-07	0.098	0.043
40	Leukotriene receptorsignaling pathway	20.724	5.78E-07	0.049	0.222
40	CART signaling pathway	20.724	5.78E-07	0.049	0.222
42	MAPK signaling pathway	20.693	5.90E-07	0.085	0.055
43	Transcriptional regulation by RB/E2F	20.543	6.55E-07	0.098	0.042
44	NAD metabolism	20.468	6.89E-07	0.061	0.114
45	ERK signaling pathway	20.425	7.11E-07	0.073	0.073
46	Adenylyl Cyclase signaling pathway	20.303	7.73E-07	0.061	0.111
47	Bile acid signaling pathway	20.141	8.65E-07	0.061	0.109

[a] Score(p) indicates p-value of the pathway.
[b] Score(v) indicates the ratio of "Count" to total molecules associated with the loaded list.
[c] Score(c) indicates the ratio of "Count" to total molecules contained in the pathway.

21 day-old					
Rank	Name	Score	Score (p) [a]	Score (v) [b]	Score (c) [c]
1	Histone demethylation	84.198	4.51E-26	0.102	0.425
2	CDK inhibitor signaling pathway	56.497	9.83E-18	0.078	0.295
3	Transcriptional regulation by RB/E2F	46.598	9.39E-15	0.108	0.095
4	Mst(Hippo) signaling pathway)	46.343	1.12E-14	0.09	0.133
5	Transcriptional regulation by androgen receptor	46.078	1.35E-14	0.078	0.178
6	p160 SRC signaling pathway	45.809	1.62E-14	0.078	0.176
7	Transcriptional regulation by SMAD	43.961	5.84E-14	0.09	0.119
8	Autophagy-related protein signaling pathway	41.063	4.35E-13	0.084	0.119
9	Transcriptional regulation by HIF	39.527	1.26E-12	0.096	0.086
10	Nucleophosmin signaling pathway	38.417	2.72E-12	0.054	0.273
11	HSP90 signaling pathway	37.887	3.93E-12	0.066	0.164
12	PAF metabolism	37.562	4.93E-12	0.042	0.5
13	Transcriptional regulation by STAT	37.276	6.01E-12	0.072	0.132
14	Bcl-2 family signaling pathway	36.157	1.31E-11	0.072	0.124
15	Sirtuin signaling pathway	34.782	3.39E-11	0.072	0.114
16	Transcriptional regulation by C/EBP	33.819	6.60E-11	0.066	0.128
17	PIN1 signaling pathway	33.172	1.03E-10	0.06	0.149
18	RSK signaling pathway	30.566	6.29E-10	0.06	0.125
19	Transcriptional regulation by High mobility group protein	29.873	1.02E-09	0.054	0.148
20	BET family signaling pathway	29.656	1.18E-09	0.054	0.145
21	Transcriptional regulation by Myc	28.838	2.08E-09	0.066	0.093
22	Transcriptional regulation by FOXO	28.827	2.10E-09	0.054	0.136
23	PSD-95 family signaling pathway	26.154	1.34E-08	0.048	0.14
24	AKT signaling pathway	25.169	2.65E-08	0.048	0.129
25	Arginine methylation	24.799	3.43E-08	0.048	0.125
26	gp130 signaling pathway	24.25	5.01E-08	0.054	0.096
27	Transcriptional regulation by CREB	23.858	6.58E-08	0.066	0.067
28	Gene regulation by microRNAs (metastasis)	23.852	6.60E-08	0.054	0.093
29	HDAC signaling pathway	23.536	8.22E-08	0.036	0.207
30	Calpain signaling pathway	23.092	1.12E-07	0.06	0.074
31	Transcriptional regulation by IRF	22.738	1.43E-07	0.054	0.085
32	2-Oxoglutarate signaling pathway	22.673	1.50E-07	0.048	0.104
32	14-3-3 signaling pathway	22.673	1.50E-07	0.048	0.104
34	Transcriptional regulation by POU domain factor	22.601	1.57E-07	0.06	0.071
35	Transcriptional regulation by BLIMP-1	22.474	1.72E-07	0.042	0.132
36	Gene regulation by microRNAs (metabolism)	22.39	1.82E-07	0.054	0.083
37	Fatty acid beta oxidation	22.096	2.23E-07	0.042	0.127
38	Transcriptional regulation by RXR	22.08	2.26E-07	0.036	0.176
39	ERK signaling pathway	21.96	2.45E-07	0.048	0.098
40	PARP signaling pathway	21.913	2.53E-07	0.042	0.125
41	Transcriptional regulation by VDR	21.618	3.11E-07	0.054	0.078
42	Transcriptional regulation by p53	21.168	4.24E-07	0.072	0.05
43	Acetylcholine metabolism	21.152	4.29E-07	0.024	0.444
44	Gene regulation by microRNAs (embryonic stem cells)	21.08	4.51E-07	0.036	0.158
45	mTOR signaling pathway	21.048	4.61E-07	0.042	0.115
46	Gene regulation by microRNAs (cancer)	21.04	4.64E-07	0.048	0.09
47	Transcriptional regulation by Ets-1/2	20.724	5.77E-07	0.042	0.111
48	MAPK signaling pathway	20.411	7.18E-07	0.054	0.07
49	Gene regulation by microRNAs (cell cycle)	20.404	7.21E-07	0.036	0.146
50	Transcriptional regulation by p73	20.259	7.97E-07	0.042	0.106

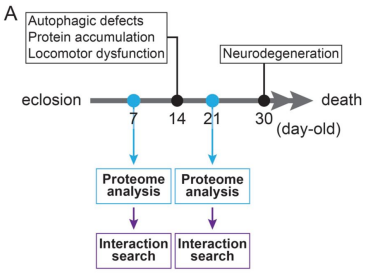

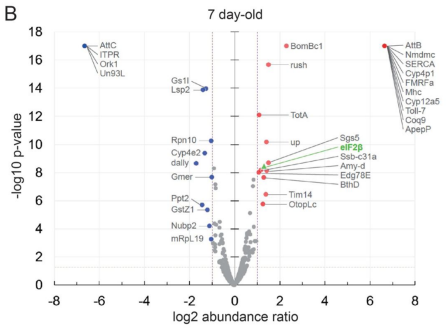

D

		Abundance Ratio : *milton* RNAi / control RNAi	
	Accession	7 day-old	21 day-old
eIF2α	P41374	1.106	0.961
eIF2β	P41375	2.465***	0.753*
eIF2γ	Q24208	0.952	0.952

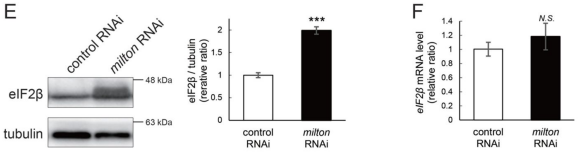

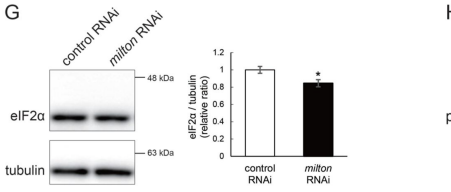

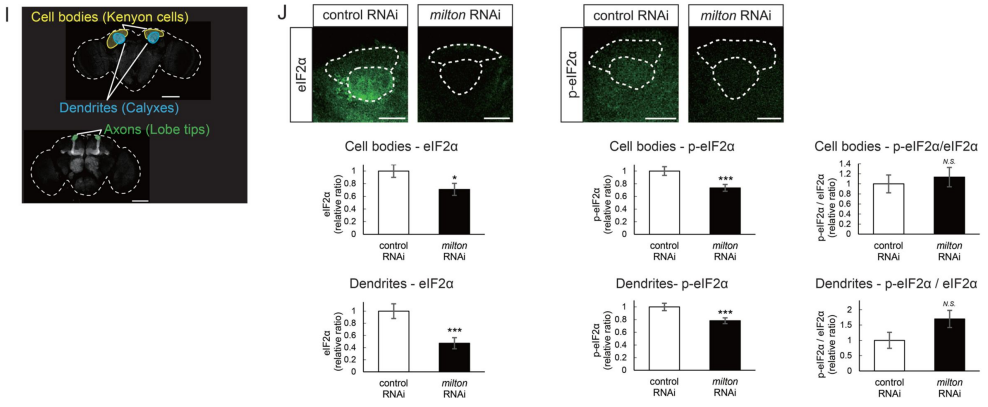

Figure 4.

***milton* knockdown upregulates eIF2β and decreases phosphorylation of eIF2α and translation**

(A) Timing of proteome analysis and phenotypes observed in *milton* knockdown flies. (B, C) Scatter plots of the $\log_2$ abundance ratio (x-axis) against the $-\log_{10}$ p-value (y-axis) of proteins at 7-day-old (B) and 21-day-old (C). (D) eIF2 subunit protein levels from proteome analysis of *milton* knockdown flies compared to those of control flies. (E) Western blotting of head extracts of flies expressing control or *milton* RNAi in neurons with an anti-eIF2β antibody. Flies were 14-day-old. Representative blots (left) and quantitation (right) are shown. Tubulin was used as a loading control. Means ± SE, n = 6. (F) *eIF2β* mRNA levels quantified by qRT-PCR. Means ± SE, n = 4, (G, H) Western blotting of head extracts with anti-eIF2α (G) and anti-p-eIF2α (H) antibodies. Flies were 14-day-old. Representative blots (left) and quantitation (right) are shown. Tubulin was used as a loading control. Means ± SE, n = 6. (I) A schematic representation of the axon (Lobe tips), the cell body region (Kenyon cells), and dendritic region (Calyxes) in the fly brain. Scale bars, 100μm. (J, K) Immunostaining with anti-eIF2α and anti-p-eIF2α antibodies. The mushroom body was identified by expression of mito-GFP. Scale bars, 20μm. The signal intensities of eIF2α and p-eIF2α in axons, dendrites, and cell bodies were quantified and are shown as ratios relative to the control. Means ± SE, n=12. *N.S.*, $p > 0.05$; *$p < 0.05$; **$p < 0.01$; ***$p < 0.005$ (Student's *t*-test).

Depletion of axonal mitochondria upregulates eIF2β and decreases phosphorylation of eIF2α

Differentially expressed proteins at 7-day-old flies may reflect alterations that are causal for autophagic defects. We noticed that the expression level of eIF2β was 2.465-fold higher in the brains of *milton* knockdown flies than in those of control flies (**Figure 4B** and **D**). Upregulation of eIF2β in the brains of *milton* knockdown flies was confirmed by western blotting. *milton* knockdown increased eIF2β protein levels more than twice (**Figure 4E**), but did not change the level of *eIF2β* mRNA (**Figure 4F**).

eIF2β is a subunit of the eukaryotic initiation factor 2 (eIF2) complex, which is critical for translation initiation and the integrated stress response (ISR)[4]. eIF2 is a heterotrimer of α, β, and γ subunits, and eIF2α is phosphorylated during the ISR[6]. As for the other subunits of eIF2 complex, proteome analysis did not detect a significant difference in the protein levels of eIF2α and eIF2γ between *milton* knockdown and control flies at 7 and 21 days (**Figure 4D**). Western blotting of brain lysates showed that *milton* knockdown reduced eIF2α levels (**Figure 4G**), while p-eIF2α levels were not significantly affected (**Figure 4H**).

To analyze local changes of eIF2α and p-eIF2α, we carried out immunostaining. We focused on the mushroom body, where axons, dendrites, and cell bodies can be easily identified (**Figure 4I**). Both eIF2α and p-eIF2α were downregulated in the cell body (Kenyon cells) and dendritic (Calyxes) regions of the brains of *milton* knockdown flies (**Figure 4J**). In axons (lobe tips), *milton* knockdown did not affect eIF2α (**Figure 4K**, $p = 0.271$) but significantly downregulated p-eIF2α (**Figure 4K**). The ratio of p-eIF2α to eIF2α was lower in the axon but not in the soma or dendritic region. These results suggest that axonal distribution of mitochondria regulate the level of overall eIF2α protein and local p-eIF2α.

Depletion of axonal mitochondria suppressed global translation

Phosphorylation of eIF2α induces conformational changes in the eIF2 complex and inhibits global translation[36]. To analyze the effects of *milton* knockdown on translation, we performed polysome gradient centrifugation to examine the level of ribosome binding to mRNA. Since p-eIF2α was downregulated, we hypothesized that *milton* knockdown would enhance translation.

However, unexpectedly, we found that *milton* knockdown significantly reduced the level of mRNAs associated with polysomes (**Figure 5A** and **B**). We also compared the level of translation between the brains of control and *milton* knockdown flies by assessing the incorporation of puromycin (**Figure 5C**). Puromycin incorporation was lower in the brains of *milton* knockdown flies than in those of control flies, while it was not statistically significant (**Figure 5C**, indicated by a bracket). These data suggest that the depletion of axonal mitochondria suppresses global translation.

eIF2β upregulation reduces the level of p-eIF2α, impairs autophagy, and decreases locomotor function

We were motivated to ask if eIF2β upregulation mediates autophagic defects caused by *milton* knockdown. If so, neuronal overexpression of *eIF2β* would also induce autophagy impairment. Neuronal overexpression of *eIF2β* increased LC3-II, while the LC3-II/LC3- I ratio was not significantly different (**Figure 6A** and **B**). Overexpression of *eIF2β* significantly increased the p62 level in the Triton X-100-soluble fraction (**Figure 6C**, 4-fold vs. control, $p < 0.005$ (1% Triton X-100)) but not in the SDS-soluble fraction (**Figure 6C**, 2-fold vs. control, $p = 0.062$ (2% SDS)), as observed in brains of *milton* knockdown flies (**Figure 2B**). These data suggest that neuronal overexpression of *eIF2β* accumulates autophagic substrates.

Since *milton* knockdown reduced the p-eIF2α level (**Figure 4K**), we asked whether an increase in eIF2β affects p-eIF2α. Neuronal overexpression of *eIF2β* did not affect the eIF2α level but significantly decreased the p-eIF2α level (**Figure 6D, E**).

Depletion of axonal mitochondria causes age-dependent decline in locomotor function[24]. We found that neuronal overexpression of *eIF2β* also caused locomotor dysfunction (**Figure 6F**). Locomotor functions were significantly impaired in those flies at 20-day-old and worsened further during aging (**Figure 6F**, compare 4-, 20-, and 30-day-old). We asked if *eIF2β* overexpression causes neurodegeneration, as depletion of axonal mitochondria in the photoreceptor neurons causes axon degeneration in an age-dependent manner[24]. *eIF2β* overexpression in photoreceptor neurons tends to increase neurodegeneration in aged flies, while it was not statistically significant (p>0.05, Figure S2).

These data indicate that an increase of eIF2β in neurons phenocopies depletion of axonal mitochondria, including suppression of autophagy and age-dependent locomotor dysfunction, and suggest that increase of eIF2β mediates these phenotypes downstream of loss of axonal mitochondria.

Lowering *eIF2β* rescues autophagic impairment and locomotor dysfunction induced by *milton* knockdown

Finally, we investigated whether suppression of eIF2β rescues autophagy impairment and locomotor dysfunction caused by neuronal knockdown of *milton*. Null mutants and flies with RNAi-mediated knockdown of *eIF2β* in neurons did not survive. Flies lacking one copy of the *eIF2β* gene survived without any gross abnormality, and the level of *eIF2β* mRNA in these flies was about 80% of that in control flies (**Figure 7A**). *eIF2β* heterozygosity did not affect the eIF2α and p-eIF2α levels (Figure S3A and B).

Neuronal knockdown of *milton* causes accumulation of autophagic substrate p62 in the Triton X-100-soluble fraction (**Figure 2B**), and we tested if lowering eIF2β ameliorates it. We found that *eIF2β* heterozygosity caused a mild increase in LC3-I levels and decreases in LC3-II levels, resulting in a significantly lower LC3-II/LC3-I ratio in *milton* knockdown flies (**Figure 7B**). *eIF2β* heterozygosity decreased the p62 level in the Triton X-100-soluble fraction in the brains of *milton*

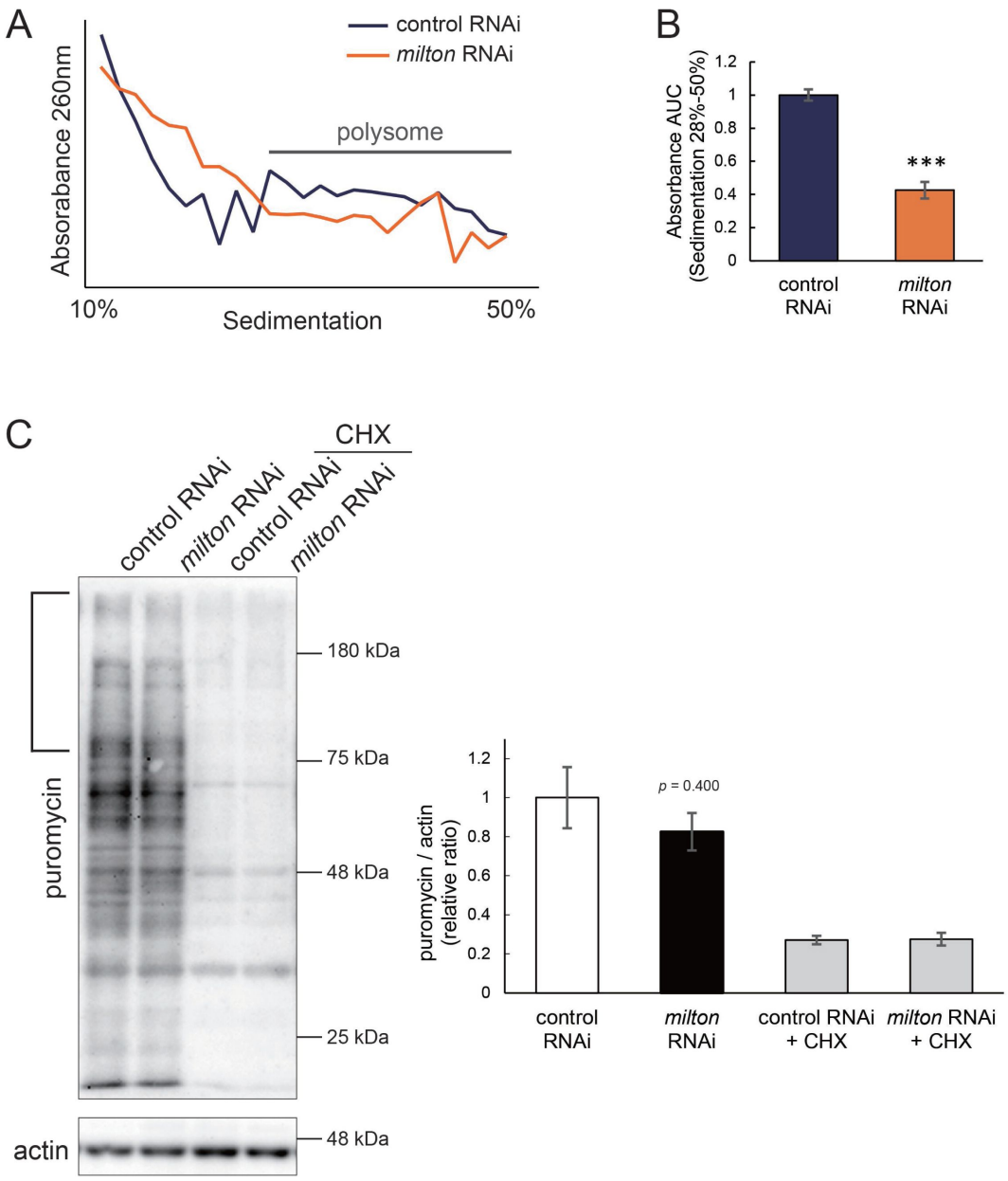

Figure 5.

***milton* knockdown suppressed global translation**

(A) Representative polysome traces of head lysates of control and *milton* knockdown flies. (B) Quantitation of polysome fraction. The relative ratio of area under the curve (AUC) of polysome fractions (sedimentation 28%-50%). Means ± SE, n = 3. ***$p < 0.005$ (Student's *t*-test) (C) Western blotting of head lysates of control and *milton* knockdown flies fed puromycin alone or puromycin and cycloheximide (CHX) with an anti-puromycin antibody. Flies were 14-day-old. Actin was used as a loading control. Representative blots (left) and quantitation (right) are shown. Means ± SE, n = 3. Student's *t*-test.

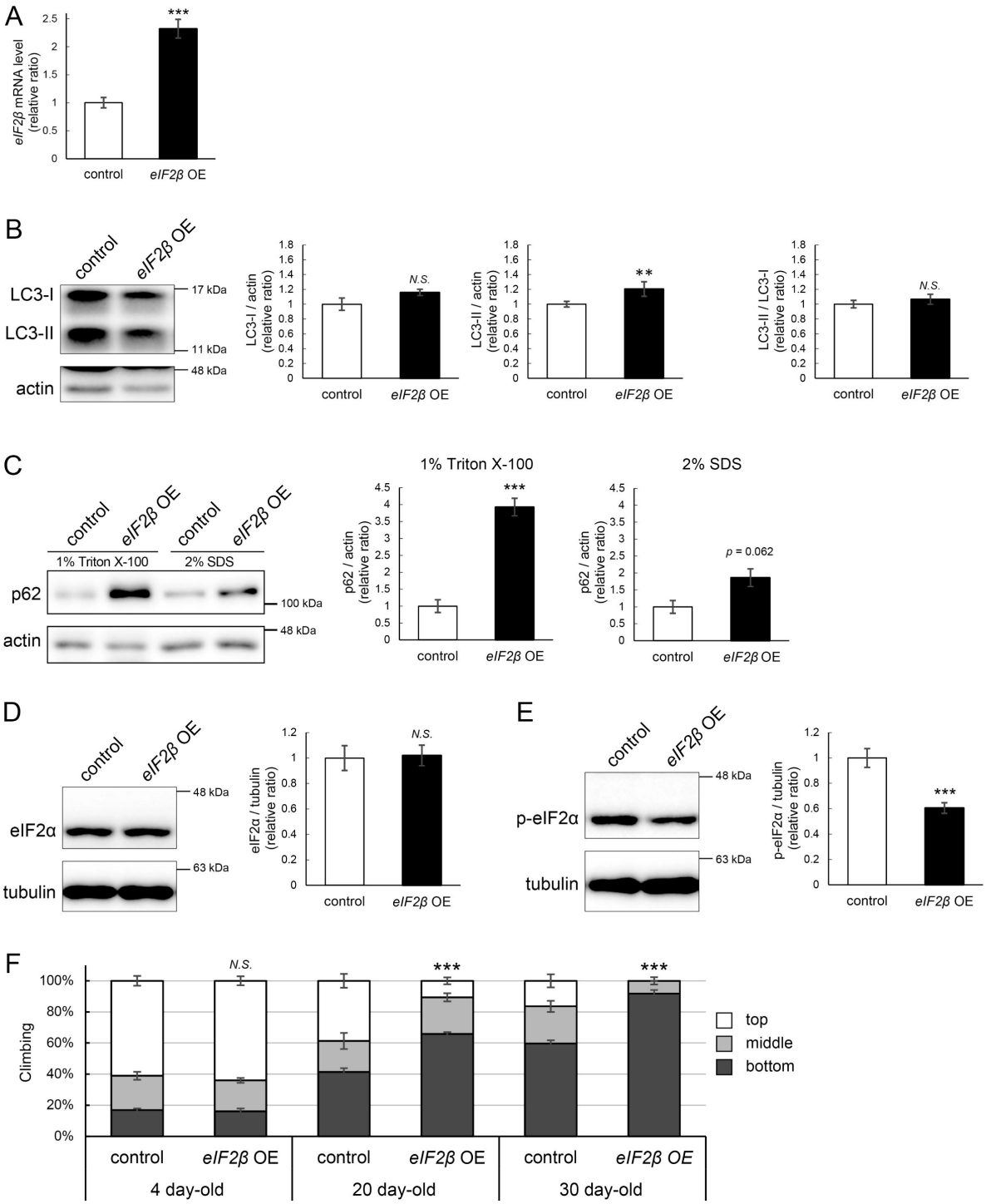

Figure 6.

eIF2β upregulation impairs autophagy and decreases locomotor function

(A) *eIF2β* mRNA levels in head extracts of flies with UAS-*eIF2β* driven by elav-Gal4 (*eIF2β* OE) or UAS-GFP driven by elav-Gal4 (control) were quantified by qRT-PCR. Flies were 2-day-old. Means ± SE, n=4. (B, C) Western blotting of head extracts with anti-LC3 (B) and anti-p62 (C) antibodies. Flies were 14-day-old. Representative blots (left) and quantitation (right) are shown. Tubulin and actin were used as loading controls. Means ± SE, n = 3 (p62), n = 5 (LC3). (D, E) Western blotting of head extracts with anti-eIF2α (D) and anti-p-eIF2α (E) antibodies. Flies were 14-day-old. Representative blots (left) and quantitation (right) are shown. Tubulin was used as a loading control. Means ± SE, n = 6. (F) Climbing assay revealed early-onset of age-dependent locomotor defects in *eIF2β*-overexpressing flies. Means ± SE, n = 5. *N.S.*, $p > 0.05$; ***$p < 0.005$ (Student's *t*-test).

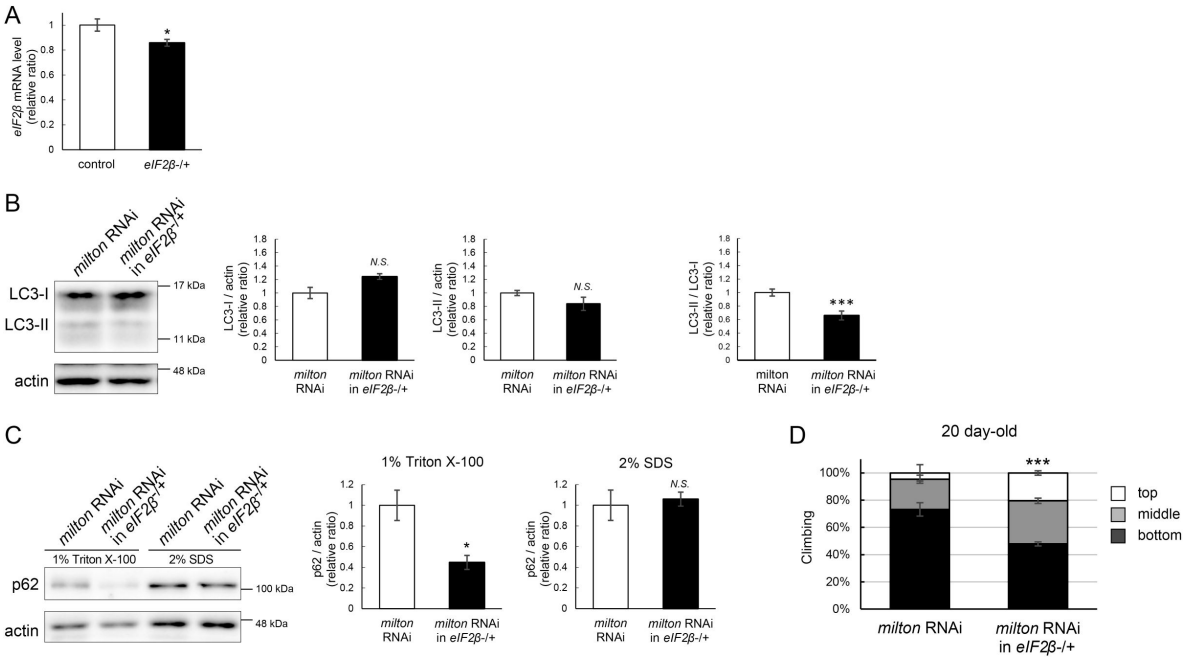

Figure 7.

Lowering *eIF2β* rescues autophagic impairment and locomotor dysfunction induced by *milton* knockdown

(A) *eIF2β* mRNA levels with one disrupted copy of the *eIF2β* gene (*eIF2β*SAstopDsRed/+ (*eIF2β* -/+)). Head extracts of flies 2–3 day-old were analyzed by qRT-PCR. Means ± SE, n = 3. (B, C) Western blotting of head extracts of flies with neuronal expression of *milton* RNAi with or without *eIF2β* heterozygosity with anti-LC3 (B) and anti-p62 (C) antibodies. Flies were 14-day-old. Representative blots (left) and quantitation (right) are shown. Actin was used as a loading control. Means ± SE, n = 5 (LC3), n = 3 (p62). (D) The climbing ability of 20-day-old flies expressing *milton* RNAi with or without *eIF2β* heterozygosity. Means ± SE, n = 15. *N.S.*, $p > 0.05$; *$p < 0.05$; ***$p < 0.005$ (Student's *t*-test).

knockdown flies (**Figure 7B**). *eIF2β* heterozygosity decreased the p62 level in the Triton X-100-soluble fraction in the brains of *milton* knockdown flies (**Figure 7C**). The p62 level in the SDS-soluble fraction, which is not sensitive to *milton* knockdown (**Figure 2B**), was not affected (**Figure 7C**). These results suggest that suppression of *eIF2β* ameliorates the impairment of autophagy caused by *milton* knockdown.

eIF2β heterozygosity also rescued locomotor dysfunction induced by *milton* knockdown. *milton* knockdown flies with *eIF2β* heterozygosity exhibited better locomotor function than *milton* knockdown alone (**Figure 7D**). The *milton* mRNA level was not increased in these flies, indicating that the rescue effect in the *eIF2β* heterozygous background was not mediated by an increase in the *milton* mRNA level (Figure S3C). These data suggest that eIF2β upregulation mediates autophagy impairment and locomotor dysfunction caused by the depletion of axonal mitochondria.

Discussion

Proteostasis perturbations trigger the formation of pathological aggregates and increase the risks of neurodegenerative diseases during aging. By using neuronal *milton* knockdown to deplete mitochondria from the axon, we provide evidence that loss of axonal mitochondria drives age-related proteostasis collapse via eIF2β (**Figure 8**). We observed declines in autophagy-mediated degradation of less-aggregated proteins and proteasome activity in *milton* knockdown flies (**Figure 2**). Accumulation of ubiquitinated proteins and changes in age-related pathways started prematurely in *milton* knockdown flies (**Figure 1** and **Table 2**). *milton* knockdown increased eIF2β and lowered eIF2α phosphorylation (**Figure 4**). Overexpression of *eIF2β* phenocopied the effects of *milton* knockdown, including reduced autophagy and accelerated age-related locomotor defects (**Figure 6**). Furthermore, lowering *eIF2β* levels suppressed the impairment of autophagy and locomotor dysfunction induced by *milton* knockdown (**Figure 7**). eIF2β protein levels are reduced at the 21-day-old; however, since a reduction in the eIF2β ameliorated *milton* knockdown-induced locomotor defects in aged flies (**Figure 7**), the reduction in eIF2β observed in the 21-day-old is not likely to negatively contribute to *milton* knockdown-induced defects. Our results suggest that mitochondrial distribution and eIF2β are part of the mechanisms constituting proteostasis.

milton knockdown causes loss of mitochondria in the axon and accumulation of mitochondria in the soma. Thus, the detrimental effects may be mediated by the accumulation of mitochondria. However, degeneration induced by *milton* knockdown is prominent in the axon and not detected in the cell body[24]. Furthermore, abnormal protein accumulation was observed in the axon (**Figure 1**), and p-eIF2α/eIF2α was decreased in the neurites but not in the soma (**Figure 4**), suggesting that proteostasis defects studied in this work are caused by depletion of mitochondria rather than accumulation of mitochondria. Further analyses to dissect the effects of *milton* knockdown on proteostasis and translation in the cell body and axon by experiments with spatial resolution would be needed.

The depletion of axonal mitochondria and accumulation of abnormal proteins are both characteristics of aged brains[37,38]. Our results suggest that the loss of axonal mitochondria is an event upstream of proteostasis collapse during aging. Neuronal knockdown of *milton* had more impact on proteostasis in young neurons than the old neurons (**Figure 1**).

Proteome analyses also showed that age-related pathways, such as immune responses, are enhanced in young flies with *milton* knockdown (**Table 2**). The reduction in axonal transport of mitochondria may be one of the triggering events of age-related changes and accelerates the onset of aging in the brain. Disruption of proteostasis is expected to contribute neurodegeneration[38],

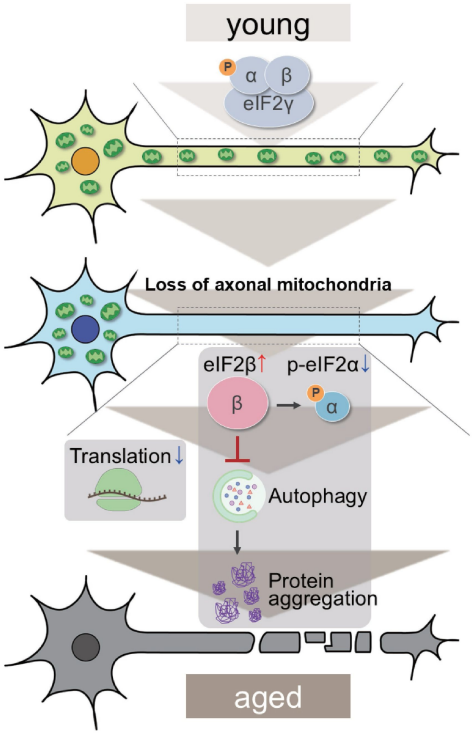

Figure 8.

Graphical abstract: the mitochondria-eIF2β axis in the axon maintains neuronal proteostasis during aging

and it would be interesting to analyze the sequence of protein accumulation and axonal degeneration in *milton* knockdown ([24,29] and **Figure 1**) in detail with higher time resolution.

Our results revealed that eIF2β regulates autophagy and maintains proteostasis during aging. eIF2β is a component of eIF2, which meditates translational regulation and ISR initiation. When ISR is activated, phosphorylated eIF2α suppresses global translation and induces translation of ATF4, which mediates transcription of autophagy-related genes[39,40]. Since ISR can positively regulate autophagy, we suspected that suppression of ISR underlies a reduction in autophagic protein degradation. We found neuronal knockdown of *milton* reduced phosphorylated eIF2α, suggesting that ISR is reduced (**Figure 4**). However, we also found that global translation was reduced (**Figure 5**). It may be possible that increased levels of eIF2β disrupt the eIF2 complex or alter its functions. The stoichiometric mismatch caused by an imbalance of eIF2 components may inhibit ISR induction. Supporting this model, we found that eIF2β upregulation reduced the levels of p-eIF2α (**Figure 6**). It is also possible that eIF2β mediates autophagy defects via mechanisms independent of ISR since eIF2β has functions independent of eIF2[41,42]. For example, suppression of *eIF2β* has been reported to slow down cancer cell growth[41]. In developing neurons, eIF2β can directly interact with the translational repressor Kra to regulate midline axon guidance[42]. However, to our knowledge, the roles of eIF2β in aging have not been reported. Our results revealed a novel function of eIF2β to maintain proteostasis during aging.

How depletion of axonal mitochondria upregulates eIF2β is currently under investigation. A major mitochondrial function is ATP production, and depletion of axonal mitochondria downregulates ATP in axons[33]. However, we found that ATP deprivation did not always suppress autophagy (**Figure 3**), suggesting it is unlikely to be involved in the mechanisms that induce eIF2β upregulation. Mitochondria also serve as signaling hubs for translation and protein degradation. Mitochondrial proteins are regulated by co-translational protein quality control, and mitochondrial damage induces translational stalling of mitochondrial outer membrane-associated *complex-I 30 kD subunit* (*C-I30*) mRNA[43]. Additionally, the mitochondrial outer membrane ubiquitin ligase MITOL (also known as MARCHF5) ubiquitinates and regulates not only mitochondrial proteins such as Mfn2[44] but also microtubule-associated[45] and endoplasmic reticulum[46] proteins. These findings indicate that mitochondria serve as local signaling centers for proteostasis maintenance, and eIF2β levels may also be regulated by mechanisms related to mitochondria.

In conclusion, our results suggest that axonal mitochondria and eIF2β form an axis to maintain constitutive autophagy. Suppression of *eIF2β* rescued autophagic defects and neuronal dysfunction upon loss of axonal mitochondria. Since eIF2β is conserved across many species, including *Drosophila* and humans, our results suggest that eIF2β may be a possible therapeutic target for aging and diseases associated with mitochondrial mislocalization.

Materials and methods

Fly stocks and husbandry

Flies were maintained in standard cornmeal medium (10% glucose, 0.7% agar, 9% cornmeal, 4% yeast extract, 0.3% propionic acid, and 0.1% n-butyl p-hydroxybenzoate) at 25°C under light–dark cycles of 12:12 h. The flies were transferred to fresh food vials for every 2–3 days. UAS-*milton* RNAi (v41508) was from VDRC and outcrossed to [w1118] for five generations in our laboratory. Transgenic fly lines carrying UAS-*luciferase* RNAi control for *milton* RNAi) was reported previously[24]. GMR-gal4, Elav-gal4, UAS-*Pfk* RNAi (Bloomington stock center #36782), UAS-*luciferase* RNAi (Bloomington stock center #31603) (control for *Pfk* RNAi), UAS-*GFP* (used for control for UAS-*eIF2β*) and UAS-*eIF2β* (eIF2β^{EY08063}, Bloomington stock center #17425) were from

the Bloomington stock center. *eIF2β* heterozygous strain (PBac{SAstopDsRed} LL07719, DGRC#142114) was from KYOTO *Drosophila* Stock Center. UAS-*mitoGFP* was a kind gift from Drs. W. M. Saxton (University of California, Santa Cruz).

Immunohistochemistry and image acquisition

Fly brains were dissected in PBS and fixed for 45 minutes in formaldehyde (4% v/v in PBS) at room temperature. After incubation in PBST containing 0.1% Triton X-100 for 10 min three times, samples were incubated for 1h at room temperature in PBST containing 1% normal goat serum (Wako, #143-06561) and then incubated overnight with the primary antibody (anti-ubiquitin antibody Ubi-1 (Thermo Fisher #13-1600) (1:50), anti-eIF2α (abcam #ab26197) (1:50) and anti-p-eIF2α (Cell signaling #3398S) (1:50)) diluted in 1% NGS/PBST at 4 °C. Samples were then washed for 10 min with PBST including 0.1% Triton X-100 three times and incubated with the secondary antibody for overnight at 4° C. Brains were mounted in Vectashield (Vectorlab Cat#H-1100) and analyzed under a confocal microscope (Nikon). Quantitative analysis was performed using ImageJ (National Institutes of Health) with maximum projection images derived from Z-stack images acquired with same settings. Puncta was identified with mean intensity and area using ImageJ. For eIF2α and p-eIF2α immunostaining, the mushroom body was detected by mitoGFP expression.

Electron microscopy

Proboscis was removed from decapitated heads, which were then incubated in primary fixative solution (2.5% glutaraldehyde and 2% paraformaldehyde in 0.1 M sodium cacodylate buffer) at R.T. for 2 hours. After washing heads with 3% sucrose in 0.1 M sodium cacodylate buffer, fly heads were post-fixed for 1 hour in secondary fixation (1% osmium tetroxide in 0.1 M sodium cacodylate buffer) on ice. After washing with H_2O, heads were dehydrated with ethanol and infiltrated with propylene oxide and Epon mixture (TAAB and Nissin EM) for 3 hours. After infiltration, specimens were embedded with an Epon mixture at 70°C for 2~3 days. Thin sections (70 nm) of laminas were collected on copper grids. The sections were stained with 5% uranyl acetate in 50% ethanol and Reynolds' lead citrate solution. Electron micrographs were obtained with a CCD Camera mounted on a JEM-1400 plus electron microscope (Jeol Ltd.). Quantitation was performed using ImageJ (National Institutes of Health).

SDS–PAGE and immunoblotting

Western blotting was performed as reported previously[24]. Briefly, heads of 10-20 *Drosophila* were homogenized with SDS-Tris-Glycine sample buffer (0.312M Tris, 5% SDS, 8% glycerol, 0.0625% BPB, 10% β-mercaptoethanol, 10μg/mL leupeptin, 0.4 μM Pefabloc, 10mM β-glycerphosphate, 10mM NaF) and after boiling at 95°C for 2 minutes, it was centrifuged at 13,200 rpm, and the supernatant was used as a sample. For p62 western blot, fly heads were homogenized with 1% PBST and after centrifugation at 13,200 rpm, the supernatant was mixed 1:1 SDS-Tris-Glycine sample buffer, and boiled at 95 °C for 2 minutes. The pellet was dissolved with 2% SDS in PBS, then centrifuged again at 13,200 rpm. The supernatant was mixed 1:1 SDS-Tris-Glycine sample buffer and then boiled at 95 °C for 2 minutes. SDS–PAGE for western blotting was performed using 15%(w/v) (LC3), 7.5%(w/v) (p62), 10% (w/v) (eIF2α, β, and p-eIF2α) polyacrylamide gels. After electrophoresis, they were transferred to PVDF membrane (Merck Millipore) using a transfer device (BIO-RAD). After transfer, the membrane was blocked with 5% skim milk/TBST (50 mM Tris (pH 7.5), 0.15 M NaCl, 0.05% Tween20) for 1 hour and incubated with primary antibody listed below overnight at 4 °C. Membranes were rinsed twice with TBST containing 0.65M NaCl and once with TBST containing 0.15M NaCl. After incubation with the secondary antibody at room temperature for 1 hour, membranes were rinsed twice with TBST containing 0.65M NaCl and once with TBST containing 0.15M NaCl. After incubation with Immobilon Western Chemiluminescent HRP Substrate (Merck Millipore), chemiluminescent signals were detected with Fusion FX (Vilber). Experiments were repeated at least 3 times with independent cohorts of flies. Primary antibodies: anti-LC3 antibody Atg8 (Merck Millipore

#ABC975) (1:1000), anti-p62 antibody Ref2P (abcam #ab178440) (1:750), anti-eIF2β antibody (1:1500), anti-eIF2α antibody (abcam #ab26197) (1:1000), anti-p-eIF2α antibody (Cell signaling #3398S) (1:2000), anti-actin antibody (SIGMA A2066) (1:3000) and anti-β tubulin antibody (Sigma #T9026) (1:800,000). Polyclonal anti-eIF2β antibody was raised against a synthetic peptide (CGLEDDTKKEDPQDEA) corresponding to the C-terminal residues 29-43 of *Drosophila* eIF2β (1:1500).

Secondary antibodies: Peroxidase-conjugated goat anti-mouse IgG antibody (Dako #P0447) (1:2000), peroxidase-conjugated pig anti-rabbit IgG antibody (Dako #P0399) (1:2000)

Proteasome assay

Heads from ten flies were homogenized in 150 µl of buffer B (25 mM Tris-HCl [pH 7.5], 2 mM ATP, 5 mM MgCl2, and 1 mM dithiothreitol). Proteasome peptidase activity in the lysates was measured with a synthetic peptide substrate, succinyl-Leu-Leu-Val-Tyr-7-amino-4-methyl-coumarin (Suc-LLVY-AMC) (Cayman). Luminescence was measured on a multimode plate reader 2300 Enspire (PerkinElmer). Experiments were repeated at least 3 times with independent cohorts of flies.

ATP assay

Heads from the 10 flies were homogenized in 50 µl of 6 M guanidine-HCl in extraction buffer (100 mM Tris and 4 mM EDTA, pH 7.8) to inhibit ATPases. Samples were boiled for 5 min and centrifuged. The supernatant was diluted 4% with extraction buffer and mixed with a reaction solution (ATP Determination kit, Invitrogen). Luminescence was measured on a multimode plate reader 2300 Enspire (PerkinElmer). The relative ATP levels were calculated by dividing the luminescence by the total protein concentration, which was determined by the Bradford method. Experiments were repeated at least 3 times with independent cohorts of flies.

Proteomic assay and pathway analysis

Sample preparation

Heads from the 35 flies were homogenized in 110 µl of extraction buffer (0.25% RapiGest SF, 50mM ammonium bicarbonate, 10mM dithiothreitol, 10µg/mL leupeptin, 0.4 µM Pefabloc, 10mM β-glycerphosphate, 10mM NaF). Homogenized samples were centrifuged and boiled for 5 min. After quantification of the protein concentration using a Pierce® 660 nm Protein Assay (Thermo Fisher Scientific), 10 µg proteins from each sample were reduced using 5 mM tris (2-carboxyethyl) phosphine hydrochloride (TCEP-HCl; Thermo Fisher Scientific) at 60°C for 1 h, alkylated using 15 mM iodoacetamide (Fujifilm Wako Pure Chemical, Osaka, Japan) at room temperature for 30 min, and then digested using 1.5 µg Trypsin Gold (Mass Spectrometry Grade; Promega, Madison, WI, USA) at 37°C for 17 h. The digests were acidified by the addition of trifluoroacetic acid (TFA), incubated at 37°C for 30 min, and then centrifuged at 17,000 ×*g* for 10 min to remove the RapiGest SF. The supernatants were collected and desalted using MonoSpin™ C18 (GL Sciences, Tokyo, Japan). The resulting eluates were concentrated *in vacuo*, dissolved in 2% MeCN containing 0.1% formic acid (FA), and subjected to LC-MS/MS analysis.

LC-MS/MS analysis and database search

LC-MS/MS analyses were performed on an Ultimate 3000 RSLCnano system (Thermo Fisher Scientific) coupled to a Q Exactive hybrid quadrupole-Orbitrap mass spectrometer (Thermo Fisher Scientific) equipped with a nano electron spray ionization (ESI) source. The LC system was equipped with a trap column (C18 PepMap 100, 0.3 × 5 mm, 5 µm, Thermo Fisher Scientific) and an analytical column (NTCC-360/75-3-125, Nikkyo Technos, Tokyo, Japan). Peptide separation was performed using a 90-min gradient of water/0.1% FA (mobile phase A) and MeCN/0.1% FA (mobile phase B) at a flow rate of 300 nL/min. Elution was performed as follows: 0–3 min, 2% B; 3–93 min,

2%–40% B; 93–95 min, 40%–95% B; 95–105 min, 95% B; 105–107 min, 95%–2% B; and 107–120 min, 2% B. The mass spectrometer was operated in data-dependent acquisition mode. The MS parameters were as follows: spray voltage, 2.0 kV; capillary temperature, 275°C; S-lens RF level, 50; scan type, full MS; scan range, *m/z* 350–1500; resolution, 70,000; polarity, positive; automatic gain control target, 3×10^6; and maximum injection time, 100 msec. The MS/MS parameters were as follows: resolution, 17,500; automatic gain control target, 1×10^5; maximum injection time, 60 msec; normalized collision energy (NCE), 27; dynamic exclusion, 15 sec; loop count, 10; isolation window, 1.6 *m/z*; charge exclusion: unassigned, 1 and ≥8; and injection volume, 1 µL (containing 0.5 µg protein). Measurements were made in duplicate for each sample.

The identification of proteins and label-free quantification (LFQ) of the detected peptides were performed using Proteome Discoverer software ver. 2.4 (Thermo Fisher Scientific). The analytical parameters used for the database search were as follows: parent mass error tolerance, 10.0 ppm; fragment mass error tolerance, 0.02 Da; search engine, sequest HT; protein database, Drosophila melanogaster (Fruit fly: SwissProt Tax ID=7227); enzyme name, trypsin (full); maximum number of missed cleavages, 2; dynamic modification, oxidation (methionine), phosphorylation (serine, threonine, tyrosine), acetyl (lysine), GG (lysine); N-terminal modification, Met-loss (methionine), and Met-loss+acetyl (methionine); static modification, carbamidomethylation (cysteine) and FDR confidence, High < 0.01, 0.01 ≤ Medium < 0.05, 0.05 ≤ Low. The parameters for LFQ were as follows: precursor abundance, based on area; and normalization mode, total peptide amount.

The abundance ratio of *milton* RNAi to control RNAi at 7 or 21 day-old was calculated. We considered proteins with an abundance ratio of ≥2.0 or ≤ 0.5 and an ANOVA *P*-value of < 0.05 based on volcano plots to be differentially expressed of *milton* RNAi. To extract molecular networks biologically relevant to the proteins that are differentially expressed in *milton* RNAi, pathway analysis was performed using KeyMolnet (KM Data Inc., Tokyo, Japan).

RNA extraction and quantitative real-time PCR analysis

Heads from more than 25 flies were mechanically isolated, and total RNA was extracted using ISOGEN (NipponGene) followed by reverse-transcription using PrimeScript RT reagent kit (Takara). The resulting cDNA was used as a template for PCR with THUNDERBIRD SYBR qPCR mix (TOYOBO) on a Thermal Cycler Dice real-time system TP800 (Takara). Expression of genes of interest was standardized relative to rp49. Relative expression values were determined by the ΔΔCT method (Livak and Schmittgen, 2001). Experiments were repeated three times, and a representative result was shown.

Primers were designed using DRSC FlyPrimerBank (Harvard Medical School). Primer sequences are shown below;

- *eIF2β* for 5'-GGACGACGACAAGAGCGAAG-3'
- *eIF2β* rev 5'-CGGTCGCATCACGAACTTTG-3'
- *milton* for 5'-GGCTTCAGGGCCAGGTATCT-3'
- *milton* rev 5'-GCCGAACTTGGCTGACTTTG-3'
- *Actin* for 5'-TGCACCGCAAGTGCTTCTAA-3'
- *Actin* rev 5'-TGCTGCACTCCAAACTTCCA-3'
- *rp49* for 5'-GCTAAGCTGTCGCACAAATG-3'
- *rp49* rev 5'-GTTCGATCCGTAACCGATGT-3'

Polysome gradient centrifugation

30 heads were homogenized in 150 µl of lysis buffer (25 mM Tris pH 7.5, 50 mM MgCl2, 250 mM NaCl, 1 mM DTT, 0.5 mg/ml cycloheximide, 0.1 mg/ml heparin). The lysates were centrifuged at 13,200 rpm at 4 °C for 5 minutes, and the supernatant was collected. The samples containing 38µg

of RNA was layered gently on top of a 10–50% w/w sucrose gradient (50 mM Tris pH 7.5, 50 mM MgCl2, 250 mM NaCl, 0.1 mg/ml heparin, 0.5 mg/ml cycloheximide in 5 ml polyallomer tube) and centrifuged at 37,000 rpm at 4°C for 150 minutes in a himac CP-NX ultracentrifuge using a P50AT rotor. Samples were fractionated from top to bottom, and absorbance at OD260 nm was analyzed by a Plate reader (EnSpire). Experiments were repeated at least 3 times with independent cohorts of flies.

Puromycin analysis

13-day-old flies were starved for 6 hr and fed 600 µM puromycin (Sigma) or 600 µM puromycin/35 mM cycloheximide (Sigma) in 5% sucrose solution for 20 hr. Incorporated puromycin was quantified by western blot with anti-puromycin antibody and normalized with actin. Experiments were repeated at least 3 times with independent cohorts of flies.

Histological analysis

Fly heads were fixed in Bouin's fixative solution for 48 h at room temperature, incubated for 24 h in 50 mM Tris/150 mM NaCl, and embedded in paraffin. Serial sections (7 µm thickness) through the entire heads were stained with hematoxylin and eosin and examined by bright-field microscopy. Images of the sections that include the lamina were captured with Keyence microscope BZ-X700 (Keyence), and the vacuole area was measured using ImageJ (National Institutes of Health).

Climbing assay

The climbing assay was performed as previously described[24]. Flies were placed in an empty plastic vial (2.5 cm in diameter × 10 cm in length). The vial was gently tapped to knock the flies to the bottom, and the number of flies reached to the top, middle and bottom areas of the vials in 10 s was counted. Experiments were repeated 10 times, and the mean percentage of flies in each area and standard deviations were calculated. Experiments were repeated with independent cohorts more than three times, and a representative result was shown.

Statistics

The number of replicates, what n represents, precision measurements, and the meaning of error bars are indicated in Figure Legends. Data are shown as means ± SEM. For pairwise comparisons, Student's t-test was performed with Microsoft Excel (Microsoft). For multiple comparisons, data were analyzed using one-way ANOVA with Tukey's HSD multiple-comparisons test in the GraphPad Prism 6.0 software (GraphPad Software, Inc., La Jolla, CA). Results with a p-value of less than 0.05 were considered to be statistically significant.

Data Availability

The datasets used and/or analyzed during the current study are available from the corresponding author upon request.

Acknowledgements

The authors thank the Bloomington stock center; TRiP at Harvard Medical School (NIH/NIGMS R01-GM084947); the Kyoto Drosophila Stock Center and the Vienna Drosophila RNAi Center for fly stocks. The authors thank Dr. Masayuki Miura from Department of Pharmaceutical Science, University of Tokyo, for proteasome activity assay protocol; Dr. Shin-ichi Hisanaga from the Department of Biological Sciences, Tokyo Metropolitan University, for critical comments; Dr. Taro

Saito, Dr. Akiko Asada from the Department of Biological Sciences, Tokyo Metropolitan University, Dr. Michiko Sekiya from Department of Alzheimer's Disease Research, National Center for Geriatrics and Gerontology, and Dr. Seiji Watanabe, Dr. Koji Yamanaka from Department of Neuroscience and Pathobiology, Research Institute of Environmental Medicine, Nagoya University for technical supports.

Additional information

Funding

This work was supported by the Sasakawa Scientific Research Grant (2021-4087) (to K.S.), the Takeda Science Foundation (to KA), Hoansha foundation grant (to KA), a research award from the Japan Foundation for Aging and Health (to KA), the Novartis Foundation (Japan) for the promotion of Science (to KA), a Grant-in-Aid for Scientific Research on Challenging Research (Exploratory) [JSPS KAKENHI Grant number 19K21593] (to KA), NIG-JOINT (National Institute of Genetics, 71A2018, 25A2019) (to K.A.) and TMU strategic research fund for social engagement (to KA).

Author contributions

K.S. and K.A. designed the experiments, interpreted the data, and wrote the manuscript; K.S., Y.M., K.M.I and E.S. conducted the experiments, and K.S., Y.M., E.S., and K.A. analyzed the data. All authors read and approved the manuscript.

Additional files

Figure S1. *Ubiquitinated proteins in brains with neuronal knockdown of milton at 1-day-old. Brains dissected at 1-day-old were immunostained with an antibody against ubiquitin. Representative images (left) and quantitation of the number of ubiquitin-positive puncta (right) are shown. Scale bars of hemibrains, 100 μm, Means ± SE, n = 8. N.S., p > 0.05 (Student's t-test).*

Figure S2. *Histology analysis of fly heads with eIF2β overexpression. The morphology of the eye with eIF2β overexpression. The dotted lines indicate the retina. Vacuoles are indicated by arrows. Representative images (left) and quantification of vacuole area (right). The flies were 40-day-old. Means ± SE, n = 5-13 N.S., p > 0.05 (Student's t-test).*

Figure S3. *Lowering the eIF2β level does not affect the levels of eIF2α and p-eIF2α. (A, B) Blotting was performed with anti-eIF2α (A) and anti-p-eIF2α (B) antibodies. Flies were 14-day-old. Representative blots (left) and quantitation (right) are shown. Tubulin was used as a loading control. Means ± SE, n = 6. (C) eIF2β gene disruption does not affect the knockdown efficiency of milton. milton mRNA levels in head extracts were quantified by qRT-PCR. Flies were 2-day-old. Means ± SE, n = 3. N.S., p > 0.05; *p < 0.05 (Student's t-test).*

Supplemental Table

References

1. Yerbury J.J., Ooi L., Dillin A., Saunders D.N., Hatters D.M., Beart P.M., Cashman N.R., Wilson M.R., Ecroyd H 2016) **Walking the tightrope: proteostasis and neurodegenerative disease** *J. Neurochem* **137**:489–505 https://doi.org/10.1111/jnc.13575

2. Hetz C 2021) **Adapting the proteostasis capacity to sustain brain healthspan** *Cell* **184**:1545–1560 https://doi.org/10.1016/j.cell.2021.02.007

3. Balch W.E., Morimoto R.I., Dillin A., Kelly J.W 2008) **Adapting proteostasis for disease intervention** *Science* **319**:916–919 https://doi.org/10.1126/science.1141448

4. Kimball S.R 1999) **Eukaryotic initiation factor eIF2** *Int J Biochem Cell Biol* **31**:25–29 https://doi.org/10.1016/s1357-2725(98)00128-9

5. Jackson R.J., Hellen C.U., Pestova T.V 2010) **The mechanism of eukaryotic translation initiation and principles of its regulation** *Nat. Rev. Mol. Cell Biol* **11**:113–127 https://doi.org/10.1038/nrm2838

6. Pakos-Zebrucka K., Koryga I., Mnich K., Ljujic M., Samali A., Gorman A.M 2016) **The integrated stress response** *EMBO Rep* **17**:1374–1395 https://doi.org/10.15252/embr.201642195

7. Kroemer G., Marino G., Levine B 2010) **Autophagy and the integrated stress response** *Mol. Cell* **40**:280–293 https://doi.org/10.1016/j.molcel.2010.09.023

8. Nandi D., Tahiliani P., Kumar A., Chandu D 2006) **The ubiquitin-proteasome system** *J Biosci* **31**:137–155 https://doi.org/10.1007/BF02705243

9. Glick D., Barth S., Macleod K.F 2010) **Autophagy: cellular and molecular mechanisms** *J. Pathol* **221**:3–12 https://doi.org/10.1002/path.2697

10. Vargas J.N.S., Hamasaki M., Kawabata T., Youle R.J., Yoshimori T 2023) **The mechanisms and roles of selective autophagy in mammals** *Nat. Rev. Mol. Cell Biol* **24**:167–185 https://doi.org/10.1038/s41580-022-00542-2

11. Aman Y., Schmauck-Medina T., Hansen M., Morimoto R.I., Simon A.K., Bjedov I., Palikaras K., Simonsen A., Johansen T., Tavernarakis N., et al. 2021) **Autophagy in healthy aging and disease** *Nat Aging* **1**:634–650 https://doi.org/10.1038/s43587-021-00098-4

12. Ross C.A., Poirier M.A 2004) **Protein aggregation and neurodegenerative disease** *Nat. Med* **10**:S10–17 https://doi.org/10.1038/nm1066

13. Rubinsztein D.C., Marino G., Kroemer G 2011) **Autophagy and aging** *Cell* **146**:682–695 https://doi.org/10.1016/j.cell.2011.07.030

14. Vos M., Lauwers E., Verstreken P 2010) **Synaptic mitochondria in synaptic transmission and organization of vesicle pools in health and disease** *Front Synaptic Neurosci* **2** https://doi.org/10.3389/fnsyn.2010.00139

15. Cheng A., Hou Y., Mattson M.P 2010) **Mitochondria and neuroplasticity** *ASN Neuro* **2** https://doi.org/10.1042/AN20100019

16. Hollenbeck P.J., Saxton W.M 2005) **The axonal transport of mitochondria** *J. Cell Sci* **118**:5411–5419 https://doi.org/10.1242/jcs.02745

17. Takihara Y., Inatani M., Eto K., Inoue T., Kreymerman A., Miyake S., Ueno S., Nagaya M., Nakanishi A., Iwao K., et al. 2015) **In vivo imaging of axonal transport of mitochondria in the diseased and aged mammalian CNS** *Proc Natl Acad Sci U S A* **112**:10515–10520 https://doi.org/10.1073/pnas.1509879112

18. Milde S., Adalbert R., Elaman M.H., Coleman M.P 2015) **Axonal transport declines with age in two distinct phases separated by a period of relative stability** *Neurobiol. Aging* **36**:971–981 https://doi.org/10.1016/j.neurobiolaging.2014.09.018

19. Vagnoni A., Hoffmann P.C., Bullock S.L 2016) **Reducing Lissencephaly-1 levels augments mitochondrial transport and has a protective effect in adult Drosophila neurons** *J. Cell Sci* **129**:178–190 https://doi.org/10.1242/jcs.179184

20. Morsci N.S., Hall D.H., Driscoll M., Sheng Z.H 2016) **Age-Related Phasic Patterns of Mitochondrial Maintenance in Adult Caenorhabditis elegans Neurons** *J. Neurosci* **36**:1373–1385 https://doi.org/10.1523/JNEUROSCI.2799-15.2016

21. Adalbert R., Coleman M.P 2013) **Review: Axon pathology in age-related neurodegenerative disorders** *Neuropathol. Appl. Neurobiol* **39**:90–108 https://doi.org/10.1111/j.1365-2990.2012.01308.x

22. Duncan J.E., Goldstein L.S 2006) **The genetics of axonal transport and axonal transport disorders** *PLoS Genet* **2** https://doi.org/10.1371/journal.pgen.0020124

23. Chen H., Chan D.C 2009) **Mitochondrial dynamics--fusion, fission, movement, and mitophagy--in neurodegenerative diseases** *Hum. Mol. Genet* **18**:R169–176 https://doi.org/10.1093/hmg/ddp326

24. Iijima-Ando K., Sekiya M., Maruko-Otake A., Ohtake Y., Suzuki E., Lu B., Iijima K.M 2012) **Loss of axonal mitochondria promotes tau-mediated neurodegeneration and Alzheimer's disease-related tau phosphorylation via PAR-1** *PLoS Genet* **8** https://doi.org/10.1371/journal.pgen.1002918

25. Lopez-Domenech G., Higgs N.F., Vaccaro V., Ros H., Arancibia-Carcamo I.L., MacAskill A.F., Kittler J.T 2016) **Loss of Dendritic Complexity Precedes Neurodegeneration in a Mouse Model with Disrupted Mitochondrial Distribution in Mature Dendrites** *Cell Rep* **17**:317–327 https://doi.org/10.1016/j.celrep.2016.09.004

26. Guo X., Macleod G.T., Wellington A., Hu F., Panchumarthi S., Schoenfield M., Marin L., Charlton M.P., Atwood H.L., Zinsmaier K.E 2005) **The GTPase dMiro is required for axonal transport of mitochondria to Drosophila synapses** *Neuron* **47**:379–393 https://doi.org/10.1016/j.neuron.2005.06.027

27. Glater E.E., Megeath L.J., Stowers R.S., Schwarz T.L 2006) **Axonal transport of mitochondria requires milton to recruit kinesin heavy chain and is light chain independent** *J. Cell Biol* **173**:545–557 https://doi.org/10.1083/jcb.200601067

28. Stowers R.S., Megeath L.J., Gorska-Andrzejak J., Meinertzhagen I.A., Schwarz T.L 2002) **Axonal transport of mitochondria to synapses depends on milton, a novel Drosophila protein** *Neuron* **36**:1063–1077 https://doi.org/10.1016/s0896-6273(02)01094-2

29. Iijima-Ando K., Hearn S.A., Shenton C., Gatt A., Zhao L., Iijima K 2009) **Mitochondrial mislocalization underlies Abeta42-induced neuronal dysfunction in a Drosophila model of Alzheimer's disease** *PLoS One* **4** https://doi.org/10.1371/journal.pone.0008310

30. Tonoki A., Kuranaga E., Tomioka T., Hamazaki J., Murata S., Tanaka K., Miura M 2009) **Genetic evidence linking age-dependent attenuation of the 26S proteasome with the aging process** *Mol. Cell. Biol* **29**:1095–1106 https://doi.org/10.1128/MCB.01227-08

31. Klionsky D.J., Abdel-Aziz A.K., Abdelfatah S., Abdellatif M., Abdoli A., Abel S., Abeliovich H., Abildgaard M.H., Abudu Y.P., Acevedo-Arozena A., et al. 2021) **Guidelines for the use and interpretation of assays for monitoring autophagy (4th edition)(1)** *Autophagy* **17**:1–382 https://doi.org/10.1080/15548627.2020.1797280

32. Bartlett B.J., Isakson P., Lewerenz J., Sanchez H., Kotzebue R.W., Cumming R.C., Harris G.L., Nezis I.P., Schubert D.R., Simonsen A., Finley K.D 2011) **p62, Ref(2)P and ubiquitinated proteins are conserved markers of neuronal aging, aggregate formation and progressive autophagic defects** *Autophagy* **7**:572–583 https://doi.org/10.4161/auto.7.6.14943

33. Oka M., Suzuki E., Asada A., Saito T., Iijima K.M., Ando K 2021) **Increasing neuronal glucose uptake attenuates brain aging and promotes life span under dietary restriction in Drosophila** *iScience* **24** https://doi.org/10.1016/j.isci.2020.101979

34. Zia A., Pourbagher-Shahri A.M., Farkhondeh T., Samarghandian S 2021) **Molecular and cellular pathways contributing to brain aging** *Behav Brain Funct* **17** https://doi.org/10.1186/s12993-021-00179-9

35. Haigis M.C., Yankner B.A 2010) **The aging stress response** *Mol. Cell* **40**:333–344 https://doi.org/10.1016/j.molcel.2010.10.002

36. Wek R.C 2018) **Role of eIF2alpha Kinases in Translational Control and Adaptation to Cellular Stress** *Cold Spring Harb Perspect Biol* **10** https://doi.org/10.1101/cshperspect.a032870

37. Currais A., Fischer W., Maher P., Schubert D 2017) **Intraneuronal protein aggregation as a trigger for inflammation and neurodegeneration in the aging brain** *FASEB J* **31**:5–10 https://doi.org/10.1096/fj.201601184

38. Grimm A., Eckert A 2017) **Brain aging and neurodegeneration: from a mitochondrial point of view** *J. Neurochem* **143**:418–431 https://doi.org/10.1111/jnc.14037

39. Bond S., Lopez-Lloreda C., Gannon P.J., Akay-Espinoza C., Jordan-Sciutto K.L 2020) **The Integrated Stress Response and Phosphorylated Eukaryotic Initiation Factor 2alpha in Neurodegeneration** *J. Neuropathol. Exp. Neurol* **79**:123–143 https://doi.org/10.1093/jnen/nlz129

40. B'Chir W., Maurin A.C., Carraro V., Averous J., Jousse C., Muranishi Y., Parry L., Stepien G., Fafournoux P., Bruhat A 2013) **The eIF2alpha/ATF4 pathway is essential for stress-induced autophagy gene expression** *Nucleic Acids Res* **41**:7683–7699 https://doi.org/10.1093/nar/gkt563

41. Salton G.D., Laurino C., Mega N.O., Delgado-Canedo A., Setterblad N., Carmagnat M., Xavier R.M., Cirne-Lima E., Lenz G., Henriques J.A.P., Laurino J.P 2017) **Deletion of eIF2beta lysine stretches creates a dominant negative that affects the translation and proliferation in human cell line: A tool for arresting the cell growth** *Cancer Biol Ther* **18**:560–570 https://doi.org/10.1080/15384047.2017.1345383

42. Lee S., Nahm M., Lee M., Kwon M., Kim E., Zadeh A.D., Cao H., Kim H.J., Lee Z.H., Oh S.B., et al. 2007) **The F-actin-microtubule crosslinker Shot is a platform for Krasavietz-mediated translational regulation of midline axon repulsion** *Development* **134**:1767–1777 https://doi.org/10.1242/dev.02842

43. Wu Z., Tantray I., Lim J., Chen S., Li Y., Davis Z., Sitron C., Dong J., Gispert S., Auburger G., et al. 2019) **MISTERMINATE Mechanistically Links Mitochondrial Dysfunction with Proteostasis Failure** *Mol. Cell* **75**:835–848 https://doi.org/10.1016/j.molcel.2019.06.031

44. Sugiura A., Nagashima S., Tokuyama T., Amo T., Matsuki Y., Ishido S., Kudo Y., McBride H.M., Fukuda T., Matsushita N., et al. 2013) **MITOL regulates endoplasmic reticulum-mitochondria contacts via Mitofusin2** *Mol. Cell* **51**:20–34 https://doi.org/10.1016/j.molcel.2013.04.023

45. Yonashiro R., Kimijima Y., Shimura T., Kawaguchi K., Fukuda T., Inatome R., Yanagi S 2012) **Mitochondrial ubiquitin ligase MITOL blocks S-nitrosylated MAP1B-light chain 1-mediated mitochondrial dysfunction and neuronal cell death** *Proc Natl Acad Sci U S A* **109**:2382–2387 https://doi.org/10.1073/pnas.1114985109

46. Takeda K., Nagashima S., Shiiba I., Uda A., Tokuyama T., Ito N., Fukuda T., Matsushita N., Ishido S., Iwawaki T., et al. 2019) **MITOL prevents ER stress-induced apoptosis by IRE1alpha ubiquitylation at ER-mitochondria contact sites** *EMBO J* **38** https://doi.org/10.15252/embj.2018100999

Author information

Kanako Shinno[†]
Department of Biological Sciences, Graduate School of Science, Tokyo Metropolitan University, Tokyo, Japan
ORCID iD: 0009-0002-7114-7686

[†]Present address: Department of Neuroscience and Pathobiology, Research Institute of Environmental Medicine, Nagoya University, Chikusa-Ku, Nagoya, Aichi, 464-8601, Japan

Yuri Miura
Research Team for Mechanism of Aging, Tokyo Metropolitan Institute for Geriatrics and Gerontology, Tokyo, Japan

Koichi M Iijima
Department of Alzheimer's Disease Research, National Center for Geriatrics and Gerontology, Ōbu, Japan, Department of Experimental Gerontology, Graduate School of Pharmaceutical Sciences, Nagoya City University, Nagoya, Japan

Emiko Suzuki
Department of Biological Sciences, Graduate School of Science, Tokyo Metropolitan University, Tokyo, Japan, Gene Network Laboratory, National Institute of Genetics and Department of Genetics, Mishima, Japan

Kanae Ando
Department of Biological Sciences, Graduate School of Science, Tokyo Metropolitan University, Tokyo, Japan, Department of Biological Sciences, School of Science, Tokyo Metropolitan University, Tokyo, Japan
ORCID iD: 0000-0002-3956-276X

For correspondence: k_ando@tmu.ac.jp

Editors

Reviewer #1 (Public Review):

The authors observed a decline in autophagy and proteasome activity in the context of Milton knockdown. Through proteomic analysis, they identified an increase in the protein levels of eIF2β, subsequently pinpointing a novel interaction within eIF subunits where eIF2β contributes to the reduction of eIF2α phosphorylation levels. Furthermore, they demonstrated that overexpression of eIF2β suppresses autophagy and leads to diminished motor function. It was also shown that in a heterozygous mutant background of eIF2β, Milton knockdown could be rescued. This work represents a novel and significant contribution to the field, revealing for the first time that the loss of mitochondria from axons can lead to impaired autophagy function via eIF2β, potentially influencing the acceleration of aging.

https://doi.org/10.7554/eLife.95576.2.sa2

Reviewer #2 (Public Review):

In the manuscript, the authors aimed to elucidate the molecular mechanism that explains neurodegeneration caused by the depletion of axonal mitochondria. In Drosophila, starting with siRNA depletion of Milton and Miro, the authors attempted to demonstrate that the depletion of axonal mitochondria induces the defect in autophagy. From proteome analyses, the authors hypothesized that autophagy is impacted by the abundance of eIF2β and the phosphorylation of eIF2α. The authors followed up the proteome analyses by testing the effects of eIF2β overexpression and depletion on autophagy. With the results from those experiments, the authors proposed a novel role of eIF2β in proteostasis that underlies neurodegeneration derived from the depletion of axonal mitochondria.

The manuscript has several weaknesses. The reader should take extra care while reading this manuscript and when acknowledging the findings and the model in this manuscript.

The defect in autophagy by the depletion of axonal mitochondria is one of the main claims in the paper. The authors should work more on describing their results of LC3-II/LC3-I ratio, as there are multiple ways to interpret the LC3 blotting for the autophagy assessment. Lysosomal defects result in the accumulation of LC3-II thus the LC3-II/LC3-I ratio gets higher. On the other hand, the defect in the early steps of autophagosome formation could result in a lower LC3-II/LC3-I ratio. From the results of the actual blotting, the LC3-I abundance is the source of the major difference for all conditions (Milton RNAi and eIF2β overexpression and depletion).

Another main point of the paper is the up-regulation of eIF2β by depleting the axonal mitochondria leads to the proteostasis crisis. This claim is formed by the findings from the proteome analyses. The authors should have presented their proteomic data with much thorough presentation and explanation. As in the experiment scheme shown in Figure 4A, the author did two proteome analyses: one from the 7-day-old sample and the other from the 21-day-old sample. The manuscript only shows a plot of the result from the 7-day-old sample, but that of the result from the 21-day-old sample. For the 21-day-old sample, the authors only provided data in the supplemental table, in which the abundance ratio of eIF2β from the 21-day-old sample is 0.753, meaning eIF2β is depleted in the 21-day-old sample. The authors should have explained the impact of the eIF2β depletion in the 21-day-old sample, so the reader could fully understand the authors' interpretation of the role of eIF2β on proteostasis.

https://doi.org/10.7554/eLife.95576.2.sa1

Author response:

The following is the authors' response to the original reviews.

> ***Public Reviews:***
>
> ***Reviewer #1 (Public Review):***
>
> *The authors observed a decline in autophagy and proteasome activity in the context of Milton knockdown. Through proteomic analysis, they identified an increase in the protein levels of eIF2β, subsequently pinpointing a novel interaction within eIF subunits where eIF2β contributes to the reduction of eIF2α phosphorylation levels. Furthermore, they demonstrated that overexpression of eIF2β suppresses autophagy and leads to diminished motor function. It was also shown that in a heterozygous mutant background of eIF2β, Milton knockdown could be rescued. This work represents a novel and significant contribution to the field, revealing for the first time that the loss of mitochondria from axons can lead to impaired autophagy function via eIF2β, potentially influencing the acceleration of aging. To further support the authors' claims, several improvements are necessary, particularly in the methods of quantification and the points that should be demonstrated quantitatively. It is crucial to investigate the correlation between aging and the proteins eIF2β and eIF2α.*

Thank you so much for your review and comments. We included analyses of protein levels of eIF2α, eIF2β, and eIF2γ at 7 days and 21 days (Figure 4D). The manuscript was revised as below;

Lines 242-245 'As for the other subunits of eIF2 complex, proteome analysis did not detect a significant difference in the protein levels of eIF2α and eIF2γ between *milton* knockdown and control flies at 7 and 21 days (Figure 4D).'

Reviewer #2 (Public Review):

In the manuscript, the authors aimed to elucidate the molecular mechanism that explains neurodegeneration caused by the depletion of axonal mitochondria. In Drosophila, starting with siRNA depletion of Milton and Miro, the authors attempted to demonstrate that the depletion of axonal mitochondria induces the defect in autophagy. From proteome analyses, the authors hypothesized that autophagy is impacted by the abundance of eIF2β and the phosphorylation of eIF2α. The authors followed up the proteome analyses by testing the effects of eIF2β overexpression and depletion on autophagy. With the results from those experiments, the authors proposed a novel role of eIF2β in proteostasis that underlies neurodegeneration derived from the depletion of axonal mitochondria.

The manuscript has several weaknesses. The reader should take extra care while reading this manuscript and when acknowledging the findings and the model in this manuscript.

The defect in autophagy by the depletion of axonal mitochondria is one of the main claims in the paper. The authors should work more on describing their results of LC3-II/LC3-I ratio, as there are multiple ways to interpret the LC3 blotting for the autophagy assessment. Lysosomal defects result in the accumulation of LC3-II thus the LC3-II/LC3-I ratio gets higher. On the other hand, the defect in the early steps of autophagosome formation could result in a lower LC3-II/LC3-I ratio. From the results of the actual blotting, the LC3-I abundance is the source of the major difference for all conditions (Milton RNAi and eIF2β overexpression and depletion). In the text, the authors simply state the observation of their LC3 blotting. The manuscript lacks an explanation of how to evaluate the LC3-II/LC3-I ratio. Also, the manuscript lacks an elaboration on what the results of the LC3 blotting indicate about the state of autophagy by the depletion of axonal mitochondria.

Thank you for pointing it out, and we apologize for an insufficient description of the result. We included quantitation of the levels of LC3-I and LC3-II in Figure 2A, 2D, 3D, 6B and 7B. As the reviewer pointed out, changes in the LC3-II/LC3-I ratio do not necessarily indicate autophagy defects. However, since p62 accumulation (Figure 2B, 2E, 3E, 6C, 7C in the original manuscript), these results collectively suggest that autophagy is lowered. We revised the manuscript to include this discussion as below:

Lines 174-186 ‘During autophagy progression, LC3 is conjugated with phosphatidylethanolamine to form LC3-II, which localizes to isolation membranes and autophagosomes. LC3-I accumulation occurs when autophagosome formation is impaired, and LC3-II accumulation is associated with lysosomal defects(31,32). p62 is an autophagy substrate, and its accumulation suggests autophagic defects(31,32). We found that *milton* knockdown increased LC3-I, and the LC3-II/LC3-I ratio was lower in *milton* knockdown flies than in control flies at 14-day-old (Figure 2A). We also analyzed p62 levels in head lysates sequentially extracted using detergents with different stringencies (1% Triton X-100 and 2% SDS). Western blotting revealed that p62 levels were increased in the brains of 14-day-old of *milton* knockdown flies (Figure 2B). The increase in the p62 level was significant in the Triton X-100-soluble fraction but not in the SDS-soluble fraction (Figure 2B), suggesting that depletion of axonal mitochondria impairs the degradation of less-aggregated proteins.’

Line 189-190 : ‘At 30 day-old, LC3-I was still higher, and the LC3-II/LC3-I ratio was lower, in *milton* knockdown compared to the control (Figure 2D).’

Line 199-201: ‘However, in contrast with *milton* knockdown, *Pfk* knockdown did not affect the levels of LC3-I, LC3-II or the LC3-II/LC3-I ratio (Figure 3D).’

Line 275-281: 'Neuronal overexpression of *eIF2β* increased LC3-II, while the LC3-II/LC3-I ratio was not significantly different (Figure 6A and B). Overexpression of *eIF2β* significantly increased the p62 level in the Triton X-100-soluble fraction (Figure 6C, 4-fold vs. control, $p < 0.005$ (1% Triton X-100)) but not in the SDS-soluble fraction (Figure 6C, 2-fold vs. control, $p = 0.062$ (2% SDS)), as observed in brains of *milton* knockdown flies (Figure 2B). These data suggest that neuronal overexpression of *eIF2β* accumulates autophagic substrates.'

Line 307-315: 'Neuronal knockdown of *milton* causes accumulation of autophagic substrate p62 in the Triton X-100-soluble fraction (Figure 2B), and we tested if lowering eIF2β ameliorates it. We found that *eIF2β* heterozygosity caused a mild increase in LC3-I levels and decreases in LC3-II levels, resulting in a significantly lower LC3-II/LC3-I ratio in *milton* knockdown flies (Figure 7B). *eIF2β* heterozygosity decreased the p62 level in the Triton X-100-soluble fraction in the brains of *milton* knockdown flies (Figure 7C). The p62 level in the SDS-soluble fraction, which is not sensitive to *milton* knockdown (Figure 2B), was not affected (Figure 7C). These results suggest that suppression of *eIF2β* ameliorates the impairment of autophagy caused by *milton* knockdown.'

> *Another main point of the paper is the up-regulation of eIF2β by depleting the axonal mitochondria leads to the proteostasis crisis. This claim is formed by the findings from the proteome analyses. The authors should have presented their proteomic data with much thorough presentation and explanation. As in the experiment scheme shown in Figure 4A, the author did two proteome analyses: one from the 7-day-old sample and the other from the 21-day-old sample. The manuscript only shows a plot of the result from the 7-day-old sample, but that of the result from the 21-day-old sample. For the 21-day-old sample, the authors only provided data in the supplemental table, in which the abundance ratio of eIF2β from the 21-day-old sample is 0.753, meaning eIF2β is depleted in the 21-day-old sample. The authors should have explained the impact of the eIF2β depletion in the 21-day-old sample, so the reader could fully understand the authors' interpretation of the role of eIF2β on proteostasis.*

Thank you for pointing it out. We included plots of the results of 21-day-old proteome as a part of the main figure (Figure 4C). As the reviewer pointed out, *eIF2β* protein levels are reduced at the 21-day-old. Since a reduction in the eIF2_β_ ameliorated milton knockdown-induced locomotor defects in aged flies (Figure 7D), the reduction in eIF2β observed in the 21-day-old milton knockdown flies is not likely to negatively contribute to milton knockdown-induced defects. We included this discussion in the manuscript as below:

Lines 337-341:'eIF2β protein levels are reduced at the 21-day-old; however, since a reduction in the eIF2β ameliorated *milton* knockdown-induced locomotor defects in aged flies (Figure 7), the reduction in eIF2β observed in the 21-day-old is not likely to negatively contribute to *milton* knockdown-induced defects.'

> *The manuscript consists of several weaknesses in its data and explanation regarding translation.*
>
> *(1) The authors are likely misunderstanding the effect of phosphorylation of eIF2α on translation. The P-eIF2α is inhibitory for translation initiation. However, the authors seem to be mistaken that the down-regulation of P-eIF2α inhibits translation.*

We are sorry for our insufficient explanation in the previous version. As the reviewer pointed out, it is well known that the phosphorylated form of eIF2α inhibits translation initiation. Neuronal knockdown of milton caused a reduction in p-eIF2α (Figure 4J and K), and it also lowered translation (Figure 5); the relationship between these two events is currently unclear. We do not think that a reduction in the p-eIF2α suppressed translation; rather, we

propose that the unbalance of expression levels of the components of eIF2 complexes negatively affects translation. We revised discussion sections to describe our interpretation more in detail as below:

Line 368-378: ‘eIF2β is a component of eIF2, which meditates translational regulation and ISR initiation. When ISR is activated, phosphorylated eIF2α suppresses global translation and induces translation of ATF4, which mediates transcription of autophagy-related genes(39,40). Since ISR can positively regulate autophagy, we suspected that suppression of ISR underlies a reduction in autophagic protein degradation. We found neuronal knockdown of *milton* reduced phosphorylated eIF2α, suggesting that ISR is reduced (Figure 4). However, we also found that global translation was reduced (Figure 5). It may be possible that increased levels of eIF2β disrupt the eIF2 complex or alter its functions. The stoichiometric mismatch caused by an imbalance of eIF2 components may inhibit ISR induction. Supporting this model, we found that eIF2β upregulation reduced the levels of p-eIF2α (Figure 6).’

We have revised the graphical abstract and removed the eIF2 complex since its role in the loss of proteostasis caused by milton knockdown has not been elucidated yet.

> *(2) The result of polysome profiling in Figure 4H is implausible. By 10%-25% sucrose density gradient, polysomes are not expected to be observed. The authors should have used a gradient with much denser sucrose, such as 10-50%.*

Thank you for pointing it out. It was a mistake of 10-50%, and we apologize for the oversight. It was corrected (Figure 5).

> *(3) Also on the polysome profiling, as in the method section, the authors seemed to fractionate ultra-centrifuged samples from top to bottom and then measured A260 by a plate reader. In that case, the authors should have provided a line plot with individual data points, not the smoothly connected ones in the manuscript.*

Thank you for pointing it out. We revised the graph (Figure 5).

> *(4) For both the results from polysome profiling and puromycin incorporation (Figure 4H and I), the difference between control siRNA and Milton siRNA are subtle, if not nonexistent. This might arise from the lack of spatial resolution in their experiment as the authors used head lysate for these data but the ratio of Phospho-eIF2α/eIF2α only changes in the axons, based on their results in Figure 4E-G. The authors could have attempted to capture the spatial resolution for the axonal translation to see the difference between control siRNA and Milton siRNA.*

Thank you for your comment. We agree that it would be an interesting experiment, but it will take a considerable amount of time to analyze axonal translation with spatial resolution. We will try to include such analyses in the future. For this manuscript, we revised the discussion section to include the reviewer's suggestion as below;

Lines 351-353: ‘Further analyses to dissect the effects of *milton* knockdown on proteostasis and translation in the cell body and axon by experiments with spatial resolution would be needed.’

> ***Recommendations for the authors:***
>
> ***From the Reviewing Editor:***
>
> *As the Reviewing Editor, I have read your manuscript and the associated peer reviews. I have concerns about publishing this work in its current form. I think that your*

> *manuscript cannot claim to have found a novel function of eIF2beta because of technical uncertainties and conceptual problems that should be addressed.*

Thank you so much for your review and comments. We addressed all the concerns raised by the reviewers. Point-by-point responses are listed below.

> *First, your manuscript is based partly on what appears to be a mistaken understanding of the mechanistic basis of the ISR. Specifically, eIF2 is a heterotrimeric complex of alpha, beta, and gamma subunits. When eIF2α is phosphorylated, the heterotrimer adopts a new conformation. This conformation directly binds and inhibits eIF2B, the decameric GEF that exchanges the GDP bound to the gamma subunit of the eIF2 complex for GTP. Unless I misunderstood your paper, you seem to propose that decreasing levels of phospho-eIF2α will inhibit translation, but this is backward from what we know about the ISR.*

Thank you for your insightful comment, and we are sorry for the confusion. We did not mean to propose that decreasing levels of phospho-eIF2_a_ inhibits translation. We apologize for our insufficient explanation, which might have caused a misunderstanding (Lines 312-318 in the original version). We agree with the reviewer that 'mismatch due to elevated eIF2-beta could change the behavior of the ISR'. We revised the text in the result section as follows:

Lines 259-264 (in the Result section) 'Phosphorylation of eIF2α induces conformational changes in the eIF2 complex and inhibits global translation(36). To analyze the effects of *milton* knockdown on translation, we performed polysome gradient centrifugation to examine the level of ribosome binding to mRNA. Since p-eIF2α was downregulated, we hypothesized that *milton* knockdown would enhance translation. However, unexpectedly, we found that *milton* knockdown significantly reduced the level of mRNAs associated with polysomes (Figure 5A and B).'

Lines 368-378 (in the Discussion section): 'eIF2β is a component of eIF2, which meditates translational regulation and ISR initiation. When ISR is activated, phosphorylated eIF2α suppresses global translation and induces translation of ATF4, which mediates transcription of autophagy-related genes(39,40). Since ISR can positively regulate autophagy, we suspected that suppression of ISR underlies a reduction in autophagic protein degradation. We found neuronal knockdown of *milton* reduced phosphorylated eIF2α, suggesting that ISR is reduced (Figure 4). However, we also found that global translation was reduced (Figure 5). It may be possible that increased levels of eIF2β disrupt the eIF2 complex or alter its functions. The stoichiometric mismatch caused by an imbalance of eIF2 components may inhibit ISR induction. Supporting this model, we found that eIF2β upregulation reduced the levels of p-eIF2α (Figure 6).'

> It may be possible that a stoichiometric mismatch due to elevated eIF2-beta could change the behavior of the ISR, but your paper doesn't adequately address the expression levels of all three eIF2 subunits: alpha, beta, and gamma. The proteomic data shown in Fig 4B is unconvincing on its own because the changes in the beta subunit are subtle. The Western blot in Figure 4C suggests that the KD changes the mass or mobility of the beta subunit, and most importantly, there are no Western blots measuring the levels of eIF2a, eIF2a-phospho, or eIF2-gamma.

We appreciate the reviewer's comment and agree that the stoichiometric mismatch due to elevated eIF2β may interfere with ISR. We found overexpression of eIF2β lowered p-eIF2 alpha (Figure S2 in V1), which supports this model. We included this data in the main figure in the revised manuscript (Figure 6D) and revised the text as below:

Lines 279-281: 'Since *milton* knockdown reduced the p-eIF2α level (Figure 4K), we asked whether an increase in eIF2β affects p-eIF2α. Neuronal overexpression of *eIF2β* did not affect the eIF2α level but significantly decreased the p-eIF2α level (Figure 6D, E).'

Expression data of eIF2α and eIF2γ from proteomic analyses has been extracted from proteome analyses and included as a table (Figure 4D). Western blots of phospho-eIF2a (Figure S1 in V1) in the main figure (Figure 4G). The result section was revised as below;

Lines 242-245: 'As for the other subunits of eIF2 complex, proteome analysis did not detect a significant difference in the protein levels of eIF2α and eIF2γ between *milton* knockdown and control flies at 7 and 21 days (Figure 4D).'

> ***Reviewer #1 (Recommendations For The Authors):***
>
> *L125-128: In this section, while the efficiency of Milton knockdown is referenced from a previous publication, it is necessary to also mention that the Miro knockdown has been similarly reported in the literature. Additionally, the Methods section lacks details on the Miro RNAi line used, and Table 2 does not include the genotype for Miro RNAi. This information should be included for clarity and completeness.*

Thank you for pointing it out. Knockdown efficiency with this strain has been reported (Iijima-Ando et al., PLoS Genet, 2012). We revised the text to include citation and knockdown efficiency as follows:

Lines 139-147: 'There was no significant increase in ubiquitinated proteins in *milton* knockdown flies at 1-day old, suggesting that the accumulation of ubiquitinated proteins caused by *milton* knockdown is age-dependent (Figure S1). We also analyzed the effect of the neuronal knockdown of *Miro*, a partner of milton, on the accumulation of ubiquitin-positive proteins. Since severe knockdown of *Miro* in neurons causes lethality, we used UAS-*Miro* RNAi strain with low knockdown efficiency, whose expression driven by elav-GAL4 caused 30% reduction of *Miro* mRNA in head extract(24). Although there was a tendency for increased ubiquitin-positive puncta in *Miro* knockdown brains, the difference was not significant (Figure 1B, $p>0.05$ between control RNAi and *Miro* RNAi). These data suggest that the depletion of axonal mitochondria induced by *milton* knockdown leads to the accumulation of ubiquitinated proteins before neurodegeneration occurs.'

> *L132-L136: The current phrasing in this section suggests an increase in ubiquitinated proteins for both Milton and Miro knockdowns. However, since there is no significant difference noted for Miro, it is incorrect to state an increase in ubiquitin-positive puncta. Furthermore, combining the results of Milton knockdown to claim an increase in ubiquitinated proteins prior to neurodegeneration is misleading. At the very least, the expression here needs to be moderated to accurately reflect the findings.*

Thank you for pointing it out. We revised the text as above.

> *L137-L141: Results in Figure 1 indicate that Milton knockdown leads to an increase in ubiquitinated proteins at 14 days, while Miro knockdown shows no difference from the control at either 14 or 30 days. Conversely, both the control and Miro exhibit an increase in ubiquitinated proteins with aging, but this trend does not seem to apply to Milton knockdown. This observation suggests that Milton KD may not affect the changes in protein quality control associated with aging. It implies that Milton's function might be more related to protein homeostasis in younger cells, or that changes due to aging might overshadow the effects of Milton knockdown. These interpretations should be included in the Results or Discussion sections for a more comprehensive analysis.*

Thank you for your insightful comment. We revised the text to include those points as follows:

Lines 152-153: 'These results suggest that depletion of axonal mitochondria may have more impact on proteostasis in young neurons than in old neurons.'

Lines 355-362: 'The depletion of axonal mitochondria and accumulation of abnormal proteins are both characteristics of aged brains(37,38). Our results suggest that the loss of axonal mitochondria is an event upstream of proteostasis collapse during aging. Neuronal knockdown of *milton* had more impact on proteostasis in young neurons than the old neurons (Figure 1). Proteome analyses also showed that age-related pathways, such as immune responses, are enhanced in young flies with *milton* knockdown (Table 2). The reduction in axonal transport of mitochondria may be one of the triggering events of age-related changes and accelerates the onset of aging in the brain.'

> *L143 : Please remove the erroneously included quotation mark.*

Thank you for pointing it out. We corrected it.

> *L145-L147:*
>
> *- While it is understood that Milton knockdown results in a reduction of mitochondria in axons, as reported previously and seemingly indicated in Figure 1E, this paper repeatedly refers to axonal depletion of mitochondria. Therefore, it would be beneficial to quantitatively assess the number of mitochondria in the axonal terminals located in the lamina via electron microscopy. Such quantification would robustly reinforce the argument that mitochondrial absence in axons is a consequence of Milton knockdown.*

Thank you for pointing it out. We included quantitation of the number of mitochondria in the synaptic terminals (Figure 1E).

The text and figure legend was revised accordingly:

Lines 156-157: 'As previously reported(24), the number of mitochondria in presynaptic terminals decreased in *milton* knockdown (Figure 1E).'

> *- The knockdown of Milton is known to reduce mitochondrial transport from an early stage, but what about swelling? By observing swelling at 1 day and 14 days, it may be possible to confirm the onset of swelling and discuss its correlation with the accumulation of ubiquitinated proteins.*

Quantitation of axonal swelling has also been included (Figure 1F).

We appreciate reviewer's comments on the correlation between the accumulation of ubiquitinated proteins and axonal swelling. Axonal swelling was not observed at 3-days-old (Iijima-Ando et al., PLoS Genetics, 2012), indicating that axonal swelling is an age-dependent event. Dense materials are found in swollen axons more often than in normal axons, suggesting a positive correlation between disruption of proteostasis and axonal damage. It would be interesting to analyze the time course of events further; however, we feel it is beyond the scope of this manuscript. We revised the text as below to include this discussion:

Lines 157-159: 'The swelling of presynaptic terminals, characterized by the enlargement and roundness, was not reported at 3-day-old(24) but observed at this age with about 4% of total presynaptic terminals (Figure 1F, asterisks).'

Lines 162-167: 'Dense materials are rarely found in age-matched control neurons, indicating that *milton* knockdown induces abnormal protein accumulation in the presynaptic terminals (Figure 1G and H). In *milton* knockdown neurons, dense materials are found in swollen presynaptic terminals more often than in presynaptic terminals without swelling, suggesting a positive correlation between the disruption of proteostasis and axonal damage (Figure 1G).'

Lines 362-365: 'Disruption of proteostasis is expected to contribute neurodegeneration(38), and it would be interesting to analyze the sequence of protein accumulation and axonal degeneration in *milton* knockdown ((24,29) and Figure 1) in detail with higher time resolution.'

> *L147-L151: Though Figures 1F and 1G provide qualitative representations, it is advisable to quantitatively assess whether dense materials significantly accumulate. Such quantitative analysis would be required to verify the accumulation of dense materials in the context of the study.*

Thank you for pointing it out. We included quantitation of the number of neurons with dense material (Figure 1G). We revised the manuscript as follows:

Line 161-163: 'Dense materials are rarely found in age-matched control neurons, indicating that *milton* knockdown induces abnormal protein accumulation in the presynaptic terminals (Figure 1G and H).'

> *Regarding Figure 1B, C:*
>
> *- Even though the count of puncta in the whole brain appears to be fewer than 400, the magnification of the optic lobe suggests a substantial presence of puncta. Please clarify in the Methods section what constitutes a puncta and whether the quantification in the whole brain is based on a 2D or 3D analysis. Detail the methodology used for quantification.*

Thank you for your comment. We revised the method section to include more details as below:

Lines 434-437: 'Quantitative analysis was performed using ImageJ (National Institutes of Health) with maximum projection images derived from Z-stack images acquired with same settings. Puncta was identified with mean intensity and area using ImageJ.'

> *- What about 1-day-old specimens? Does Milton knockdown already show an increase in ubiquitinated protein accumulation at this early stage? Investigating whether ubiquitin-protein accumulation is involved in aging promotion or is already prevalent during developmental stages is a necessary experiment.*

Thank you for your comment. We carried out immunostaining with an anti-ubiquitin antibody in the brains at 1-day-old. No significant difference was detected between the control and *milton* knockdown. This result has been included as Figure S1 in the revised manuscript. The result section was revised as below:

Line 136-139 'There was no significant increase in ubiquitinated proteins in *milton* knockdown flies at 1-day old, suggesting that the accumulation of ubiquitinated proteins caused by *milton* knockdown is age-dependent (Figure S1).'

> *For Figure 1E: In the Electron Microscopy section of the Methods, define how swollen axons were identified and describe the quantification methodology used.*

Thank you for your comment. Swollen axons are, unlike normal axons, round in shape and enlarged. We revised the text as below;

Lines 157-160: 'The swelling of presynaptic terminals, characterized by the enlargement and roundness, was not reported at 3-day-old(24) but observed at this age with about 4% of total presynaptic terminals (Figure 1F, asterisks).'

Lines 683-684, Figure 1 legend: 'Swollen presynaptic terminals (asterisks in (F)), characterized by the enlargement and higher circularity, were found more frequently in milton knockdown neurons.'

> *L218-L219: Throughout the text, the expression 'eIF2β is "upregulated" in response to Milton knockdown' is frequently used. However, considering the presented results, it might be more accurate to interpret that under the condition of Milton knockdown, eIF2β is not undergoing degradation but rather remains stable.*

Thank you for pointing it out. We replaced 'upregulated' with 'increased' throughout the text.

> *L234-L235: On what basis is the conclusion drawn that there is a reduction? Given that three experiments have been conducted, it would be possible and more convincing to quantify the results to determine if there is a significant decrease.*

Thank you for pointing it out. We quantified the AUC of polysome fraction and carried out statistical analysis. There is a significant decrease in polysome in *milton* knockdown, and this result has been included in Figure 5B. We revised the figure and the legend accordingly.

> *L236: 5H-> 4H*

Thank you for pointing it out, and we are sorry for the confusion. We corrected it.

> *L238-L239: Since there is no significant difference observed, it may not be accurate to interpret a reduction in puromycin incorporation.*

Thank you for pointing it out. As described above, quantification of polysome fractions showed that *milton* knockdown significantly reduce polysome (Figure 5B). We revised the manuscript as below;

Lines 263-264: 'However, unexpectedly, we found that milton knockdown significantly reduced the level of mRNAs associated with polysomes (Figure 5A and B).'

> *Figure 5D and Figure 6D: Climbing assays have been conducted, but I believe experiments should also be performed to examine whether overexpression or heterozygous mutants of eIF2β induce or suppress degeneration.*

Thank you for pointing it out. We analyzed the eyes with eIF2_β_ overexpression for neurodegeneration. Although there was a tendency of elevated neurodegeneration in the retina with eIF2_β_ overexpression, the difference between control and eIF2_β_ overexpression did not reach statistical significance (Figure S2). This result has been included as Figure S2 in the revised manuscript, and the following sentences have been included in the text:

Lines 288-293: 'We asked if *eIF2β* overexpression causes neurodegeneration, as depletion of axonal mitochondria in the photoreceptor neurons causes axon degeneration in an age-dependent manner(24). *eIF2β* overexpression in photoreceptor neurons tends to increase neurodegeneration in aged flies, while it was not statistically significant ($p>0.05$, Figure S2).'

> *L271-L272: The results in Figure 6B are surprising. I anticipated a greater increase compared to the Milton knockdown alone. While p62 appears to be reduced, it is not clear why these results lead to the conclusion that lowering eIF2β rescues autophagic impairment. Please add a discussion section to address this point.*

Thank you for pointing it out. We apologize for the unclear description of the result. Milton knockdown flies show p62 accumulation (Figure 2), and deleting one copy of *eIF2beta* in *milton* knockdown background reduced p62 accumulation (Figure 7C). We revised the text as below:

Lines 307-315: 'Neuronal knockdown of *milton* causes accumulation of autophagic substrate p62 in the Triton X-100-soluble fraction (Figure 2B), and we tested if lowering eIF2β ameliorates it. We found that *eIF2β* heterozygosity caused a mild increase in LC3-I levels and decreases in LC3-II levels, resulting in a significantly lower LC3-II/LC3-I ratio in *milton* knockdown flies (Figure 7B). *eIF2β* heterozygosity decreased the p62 level in the Triton X-100-soluble fraction in the brains of *milton* knockdown flies (Figure 7C). The p62 level in the SDS-soluble fraction, which is not sensitive to *milton* knockdown (Figure 2B), was not affected (Figure 7C). These results suggest that suppression of *eIF2β* ameliorates the impairment of autophagy caused by *milton* knockdown.'

> *L369: Please specify the source of the anti-ubiquitin antibody used.*

Thank you for pointing it out. We included the antibody information in the method section.

> *Figure 7: While the relationship between Milton knockdown and the eIF2β and eIF2α proteins has been elucidated through the authors' efforts, I would like to see an investigation into whether eIF2β is upregulated and eIF2α phosphorylation is reduced in simply aged Drosophila. This would help us understand the correlation between aging and eIF2 protein dynamics.*

Thank you for your comment. We agree that it is an important question, and we are working on it. However, we feel that it is beyond the scope of the current manuscript.

> *L645-L646: If the mushroom body is identified using mito-GFP, then include mito-GFP in the genotype listed in Supplementary Table 2.*

We are sorry for the oversight. We corrected it in Supplementary Table 2.

> *Additionally, while it is presumed that the mito-GFP signal decreases in axons with Milton RNAi, how was the lobe tips area accurately selected for analysis? Please include these details along with a comprehensive description of the quantification methodology in the Methods section.*

Thank you for your comment. Although the mito-GFP signal in the axon is weak in the *milton* knockdown neurons, it is sufficient to distinguish the mushroom body structure from the background. We revised the method section to include this information in the method section:

Line 437-438: 'For eIF2α and p-eIF2α immunostaining, the mushroom body was detected by mitoGFP expression.'

https://doi.org/10.7554/eLife.95576.2.sa0